JOURNAL OF GEOPHYSICAL RESEARCH, VOL. 101, NO. B6, PAGES 13,851–13,868, JUNE 10, 1996

Viscoplastic modeling of texture development in polycrystalline ice with a self-consistent approach: Comparison with bound estimates

Olivier Castelnau and Paul Duval

Laboratoire de Glaciologie et Géophysique de l'Environnement, CNRS, St-Martin d'Hères, France

Ricardo A. Lebensohn

Instituto de Física de Rosario, Consejo Nacional de Invastigaciones Científicas y Tecnicas, Universidad Nacional de Rosario, Rosario, Argentina

Gilles R. Canova

Laboratoire de Génie Physique et Mécanique des Matériaux, Ecole Nationale Supérieure de Physique de Grenoble, St-Martin d'Hères, France

Abstract. Ice crystals deform easily by dislocation glide on basal planes, which provides only two independent easy slip systems. The necessary slip on other systems limits the strain rate of polycrystalline ice. The preferred *c* axis orientation of ice from polar ice sheets develops as a result of intracrystalline slip. An anisotropic viscoplastic self-consistent (VPSC) approach is used for predicting texture development and mechanical behavior of polycrystalline ice. Results are compared with lower and upper bound estimations. It is assumed that ice crystals deform by basal, prismatic, and pyramidal slip. The resistance of each slip system is determined from experimental data on monocrystals and isotropic polycrystals. The VPSC model can predict the behavior of isotropic polycrystalline ice on both the macroscopic and microscopic scale. This is not the case for the lower and upper bounds. Fabrics simulated in uniaxial extension and compression are qualitatively similar for all models. However, large differences in the rate of fabric development are found. This is explained by the different interaction stiffness between grain and matrix. Fabric concentration obtained with the VPSC model for uniaxial deformation is in close agreement with those observed in polar ices. In simple shear, the single maximum fabric found in situ cannot be reproduced without an extensive (and probably unrealistic) activity of nonbasal systems. The preferential growth of grains well oriented for basal glide associated with rotation recrystallization could be at the origin of the discrepancy between model results and natural simple shear fabrics. Distorted grain shape is found to slightly slow down fabric development.

Introduction

The constitutive law of polycrystalline ice adopted for ice sheet modeling is that of an incompressible, non linear, isotropic, viscous fluid. The development of lattice preferred orientations (fabrics) as ice is transported into the depths of ice sheets has been revealed by the study of deep ice cores from Antarctica and Greenland. Owing to the very large anisotropy of ice crystals and the preponderance of intracrystalline dislocation glide in polar ice [*Pimienta and Duval*, 1987], initially isotropic ice near the surface becomes anisotropic when fabric develops, exhibiting a different viscous response to shear stress on different planes. Very large variations of strain rates with the applied stress direction have been found with both laboratory and in situ measurements [*Russell-Head and Budd*, 1979; *Duval and Le Gac*, 1982; *Gundestrup and Hansen*, 1984; *Shoji and Langway*, 1988; *Budd and Jacka*, 1989]. Such anisotropy renders the isotropic model for polar ice inadequate for ice sheet flow modeling.

Since fabrics develop with strain, the anisotropic constitutive laws must be associated with a model giving the evolution of lattice preferred orientations. Physically based modeling of plastic deformation in polycrystals is the normal way to simulate fabric development. In this paper we present results from several homogenization methods. The viscoplastic macroscopic response (i.e., of the polycrystal) is calculated by averaging microscopic responses (i.e., of grains). A microscopic constitutive relation is chosen, but the form of the macroscopic constitutive relation is not known in advance. The general assumption is that grains deform by dislocation slip only, where different resistance is attributed to each slip system. Deformation mechanisms such as diffusional creep, grain boundary sliding, and climb of basal dislocations [*Duval et al.*, 1983; *Lliboutry and Duval*, 1985] are not taken into account. Since polar ice deforms essentially by dislocation glide in basal planes, the effects of these

Paper number 96JB00412.
0148-0227/96/96JB-00412$09.00

mechanisms are expected to be very small. Furthermore, the elastic strain is neglected in the models; applications are thus restricted to testing conditions for which the imposed strain rate does not present a rapid evolution with time.

The first approach considers that the stress on each grain is equal to the macroscopic stress applied to the aggregate [*Sachs*, 1928]. This static approximation leads to a lower bound for the stress (for a specified strain rate) on both the local and global scale. The equilibrium condition within the polycrystal is fully respected, and only the softest slip systems are activated, since ice crystals exhibit a viscoplastic response. However, the deformation is necessarily incompatible.

Another simple theory was proposed by *Taylor* [1938] in which the local deformation within the polycrystal is homogeneous. Grains of different orientations deform at the same rate. This assumption, which leads to an upper bound for the stress [*Kocks*, 1970], assures the compatibility of deformations but violates stress equilibrium across grain boundaries. In order to produce any strain, activation of up to five independent slip systems is necessary. This model is not well adapted to strongly anisotropic materials. Principal applications to geological materials were presented by *Hutchinson* [1977], *Wenk et al.* [1986, 1989a, 1989b], and *Tomé et al.* [1991].

A reasonable estimate of the macroscopic flow stress can be obtained with the viscoplastic self-consistent (VPSC) theory developed by *Hutchinson* [1976] and formulated in a general framework by *Molinari et al.* [1987]. Within the formulation of *Molinari et al.*, stress and strain rate fields are calculated in the polycrystal by solving stress equilibrium and incompressibility equations. The whole polycrystal volume is discretized into small-volume elements in which the stress state is uniform. In the simplest form of the VPSC model, these small-volume elements are the grains. Effects of nearest neighbor interaction are not taken into account. Thus this model consists in regarding each grain of the polycrystal as an inclusion embedded in an infinite homogeneous equivalent medium (HEM). The behavior of the HEM, which represents that of the polycrystal, is not known in advance. This treatment leads to an interaction equation that linearly relates the deviations of local stress and strain rate with respect to the macroscopic stress and strain rate of the HEM at infinity (Figure 1). The stress and strain rate are different in each grain and depend on the crystallographic orientation, the shape of the grain, and on the polycrystal behavior. This theory, which represents a compromise between the lower and upper bounds, has been adapted to isotropic materials by *Molinari et al.* [1987] and has provided interesting results for several geological materials [*Wenk et al.*, 1989a, 1989b, 1991; *Tomé et al.*, 1991]. A VPSC approach that explicitly accounts for the plastic anisotropy of both the grains and the matrix has been developed by *Lebensohn and Tomé* [1993]. This latter model has been applied to Zr alloys [*Lebensohn and Tomé*, 1993; *Lebensohn et al.*, 1994] and also to brass, calcite, and uranium [*Lebensohn and Tomé*, 1994].

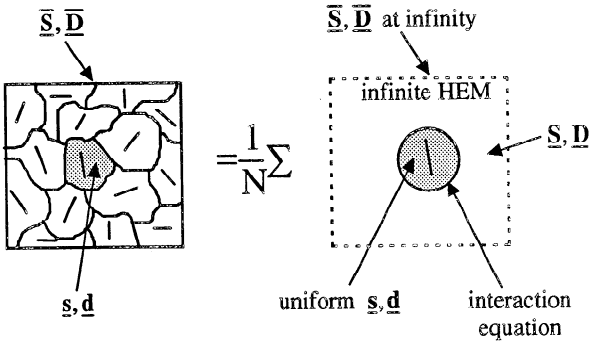

Figure 1. Calculation scheme of the VPSC model. Each grain is considered as an inclusion in a homogeneous equivalent medium (HEM), whose mechanical behavior is that of the polycrystal.

Several simple polycrystal models have been adapted to the case of ice. A general assumption is that deformation occurs by basal glide only. *Azuma and Higashi* [1985], *Fujita et al.* [1987], *Alley* [1988], and *Lipenkov et al.* [1989] have developed models for fabric development under uniaxial and biaxial deformation, for which the expression of the deformation of each grain results from a simple kinematic condition. *Azuma* [1995] has proposed an anisotropic constitutive law under uniaxial compression that takes into account the interaction between adjacent grains. This nearest neighbor interaction influences local stress and strain rate [*Becker and Panchanadeswaran*, 1995] and texture development [*Canova et al.*, 1992] and should be taken into account when rotation recrystallization is active. According to *Lliboutry and Duval* [1985], the uniform stress approximation is applicable to polar ice because incompatibilities at grain boundaries can be relieved by the grain boundary migration associated with dynamic recrystallization. This lower bound has recently been applied to fabric development in polar ice [*Van der Veen and Whillans*, 1994; *Castelnau and Duval*, 1995]. The difficulty inherent in this model is that at a given macroscopic stress, the rate of basal glide in each grain is adjusted to reproduce the response of an isotropic polycrystal. However, the behavior of crystals must also be adjusted for anisotropic ice. Consequently, the mechanical behavior of each grain is dependent on fabrics.

In this paper we apply the anisotropic viscoplastic self-consistent approach of *Lebensohn and Tomé* [1993] to fabric development in ice, where effects of grain boundary migration are not taken into account. Results are compared with calculations based on the lower and upper bounds. After a review of the deformation processes in ice, and a description of the models, we determine the resistance of each slip system from experimental data on monocrystals and isotropic polycrystals. Afterward, we compare fabric development based on these theories with fabrics observed in deep polar ices and obtained experimentally. Application to the rheology of polar ices is also discussed. With the self-consistent model, emphasis is laid on the parametrization of the grain-matrix interaction, i.e., on the possibility of imposing more or less stringent kinematic conditions on grains.

Deformation Processes of Monocrystalline and Polycrystalline Ice

The main feature of the plasticity of ice crystals is its outstanding anisotropy. For shear stresses of the order of 0.1 MPa, such as those found in active glaciers, ice deforms by basal slip. As was shown by *Duval et al.* [1983], the resistance to shear on nonbasal planes is large and can be 60

times higher than that on the basal plane. Basal slip is caused by the glide motion of 1/3 $<11\bar{2}0>$ dislocations. Very clear parallel slip lines can be observed across the crystal. Among several possibilities of nonbasal slip, the rapid glide of nonbasal edge dislocations on $(1\bar{1}00)$ prismatic planes was observed by X ray topography, using a high-power generator [*Higashi et al.*, 1985; *Ahmad and Whitworth*, 1988]. But, the rapid movement of short edge segments is trailing long screw dislocations which are dissociated on the basal plane [*Hondoh et al.*, 1990]. Therefore these basal dislocations cannot move on prismatic planes. The prismatic slip provides a mechanism for the generation of dislocations on the basal slip system, but it does not significantly contribute to the deformation of ice crystals [*Hondoh et al.*, 1990; *Shearwood and Whitworth*, 1993]. Other nonbasal slip systems were proposed by *Fukuda et al.* [1987] and *Wei and Dempsey* [1994].

During a mechanical test on a monocrystal with a constant strain rate, the stress-strain curve, after an initial yield drop caused by dislocation multiplication, becomes horizontal with no sign of work hardening up to 20% strain. Creep data for single crystals are shown in Figure 2. Almost all authors report a stress exponent for basal glide of 2±0.2, and an activation energy close to 63 kJ mol^{-1} [*Duval et al.*, 1983]. The value of the stress exponent may be explained by the linear variation of both the number of dislocation sources and the velocity of dislocations with stress. When ice crystals are loaded so that there is no resolved shear stress on the basal plane, the creep rate is at least 4 orders of magnitude lower, at a given stress, than that for basal glide. Thus the creep rate is so small that it is doubtful that it was measured accurately. The corresponding data points are shown with arrows to indicate that they represent only a lower bound for the stress or an upper bound for the strain rate.

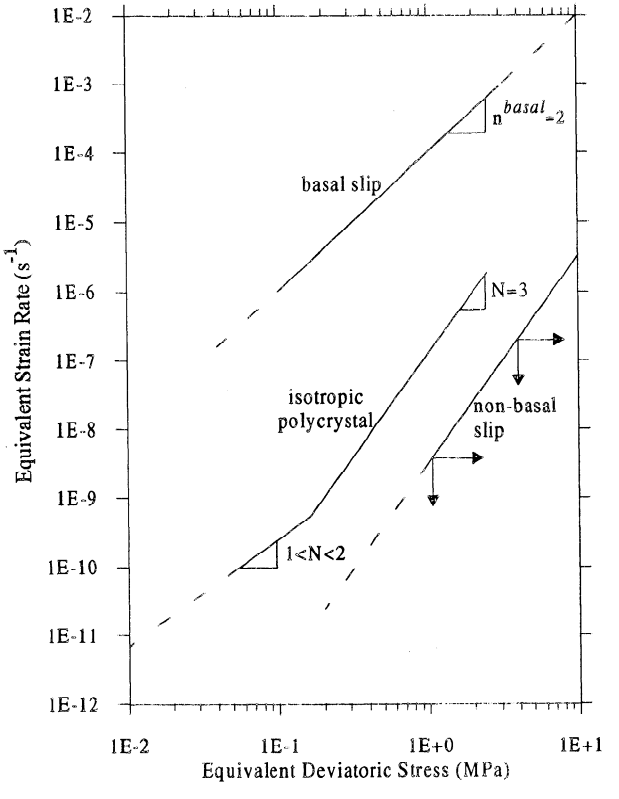

Figure 2. Steady creep behavior at -10°C of single crystals, deformed by basal or nonbasal slip, and of isotropic polycrystals. Data for single crystals and for polycrystals corresponding to N=3 are from *Duval et al.* [1983]. Data for polycrystal at lower stresses are from *Duval and Castelnau* [1995].

Creep data for isotropic polycrystalline ice are also given in Figure 2. They concern the minimum creep rate reached after a strain of about 1%. During the primary creep, strain rate decreases by more than 3 orders of magnitude [*Jacka*, 1984]. On first loading, the stress state within polycrystalline ice is almost uniform. However, owing to the very large plastic anisotropy of ice crystals, the resolved stress on the basal plane on each grain relaxes, and the load is transferred to the harder systems. As a result, an increasingly nonuniform state of internal stress develops. According to *Hutchinson* [1977], extensive plasticity of polycrystalline ice is possible with only four independent slip systems if no accomodation processes are activated. Basal slip provides two independent systems. Shear on nonbasal planes or the climb of dislocations on prismatic planes gives two additional independent systems [*Duval et al.*, 1983].

At high deviatoric stresses (higher than 0.2 MPa), the stress exponent for the polycrystal is close to 3. Nonbasal glide or climb of basal dislocations should control the strain rate. For conditions prevailing in ice sheets (stress smaller than 0.2 MPa), some laboratory and field observations support a stress exponent smaller than 2 [*Doake and Wolff*, 1985; *Pimienta and Duval*, 1987]. However, this result is the subject of discussions from several years [*Hooke*, 1981; *Budd and Jacka*, 1989]. On the other hand, diffusional creep cannot be invoked for polar ice; it yields a viscosity much higher than that deduced from both laboratory and in situ measurements and cannot be at the origin of fabrics observed in polar ice sheets. Since twinning is not observed, intracrystalline dislocation creep remains the main deformation mechanism in polycrystalline ice as long as grain size is larger than 1 mm. A sort of Harper-Dorn creep has been proposed by *Lliboutry and Duval* [1985] and *Wang* [1994] that could explain the quasi-Newtonian viscosity observed at very low stresses.

In polar ice sheets the deformation of ice is associated with three different recrystallization mechanisms. "Grain growth" driven by grain boundary energy is observed from the surface down to a depth of several hundred meters in the central parts of ice sheets. At -53°C the grain boundary migration rate is about 2×10^{-17} m^{2}s^{-1}. Coarse and interlocking grains are found in warm ice near the bedrock in Antarctica. This texture is a direct consequence of the high velocity of grain boundary migration (of about 10^{-11}m^{2}s^{-1} at -10°C) associated with "migration recrystallization" [*Pimienta and Duval*, 1989]. In situ data indicate that this recrystallization mechanism occurs only above a critical temperature close to -12°C. Between these two zones, new grains are found during progressive misorientation of subboundaries. Grain boundary migration is driven by both grain boundary and strain energies. As a result, grain size does not change significantly with depth, as was shown by *Alley et al.* [1995] for the Byrd core. This recrystallization regime is termed "rotation recrystallization" by *Guillopé and Poirier* [1979] and is associated with a low-velocity grain boundary migration [*Duval and Castelnau*, 1995]. The Harper-Dorn creep with a

Newtonian viscosity is expected at low stresses, when grain boundary migration associated with grain growth accommodates basal glide and thus impedes strain hardening. The role of these recrystallization processes in the development of lattice preferred orientations will be discussed later in connection with our numerical results.

Description of the Models

In this paper, tensors describing microscopic and macroscopic states are indicated by lowercase and capital boldface letters (**a** and **A**), respectively. Vectors are not underlined (**a**), second-order tensors are underlined once ($\underline{\mathbf{a}}$), and fourth-order tensors twice ($\underline{\underline{\mathbf{a}}}$). Tensorial, once contracted, and twice contracted products are indicated by circled cross ($\otimes$), dot (.), and colon (:), respectively. We get, for instance, for second-order tensors

$$\underline{\underline{\mathbf{C}}} = \underline{\mathbf{A}} \otimes \underline{\mathbf{B}} \Leftrightarrow C_{ijkl} = A_{ij}B_{kl}$$

$$\underline{\mathbf{C}} = \underline{\mathbf{A}}.\underline{\mathbf{B}} \Leftrightarrow C_{ik} = A_{ij}B_{jk}$$

$$C = \underline{\mathbf{A}}:\underline{\mathbf{B}} \Leftrightarrow C = A_{ij}B_{ij}$$

with the Einstein summation convention on repeated indices.

At grain level, the shear rate of a slip system s is taken as a function of the local deviatoric Cauchy stress tensor $\underline{\mathbf{s}}$ [*Hutchinson*, 1976]:

$$\dot{\gamma}^s = \dot{\gamma}_0 \left| \frac{\tau_r^s}{\tau_0^s} \right|^{n^s-1} \frac{\tau_r^s}{\tau_0^s} = \dot{\gamma}_0 \left| \frac{\underline{\mathbf{r}}^s:\underline{\mathbf{s}}}{\tau_0^s} \right|^{n^s-1} \frac{\underline{\mathbf{r}}^s:\underline{\mathbf{s}}}{\tau_0^s} \tag{1}$$

where $\dot{\gamma}_0$ is a reference shear rate, and n^s, τ_r^s and τ_0^s are respectively the inverse of the rate sensitivity factor, the resolved shear stress (RSS), and the reference resolved shear stress (RRSS) associated with system s. The Schmid tensor $\underline{\mathbf{r}}^s$ expresses the orientation of the slip system s relative to the macroscopic axes:

$$\underline{\mathbf{r}}^s = \frac{1}{2}(\mathbf{n}^s \otimes \mathbf{b}^s + \mathbf{b}^s \otimes \mathbf{n}^s), \tag{2}$$

where $\mathbf{n}^s$ and $\mathbf{b}^s$, which characterize the system s, denote the unit vector normal to the slip plane and the unit vector parallel to the Burger vector, respectively.

The constitutive law of a single crystal, which expresses its strain rate $\underline{\mathbf{d}}$, is given by a sum over all S slip systems:

$$\underline{\mathbf{d}} = \dot{\gamma}_0 \sum_{s=1}^{S} \underline{\mathbf{r}}^s \left| \frac{\underline{\mathbf{r}}^s:\underline{\mathbf{s}}}{\tau_0^s} \right|^{n^s-1} \frac{\underline{\mathbf{r}}^s:\underline{\mathbf{s}}}{\tau_0^s}. \tag{3}$$

We call $\overline{\underline{\mathbf{S}}}$ the macroscopic deviatoric Cauchy stress tensor and $\overline{\underline{\mathbf{L}}}$ the imposed macroscopic velocity gradient. The macroscopic strain rate and rotation rate tensors (noted $\overline{\underline{\mathbf{D}}}$ and $\overline{\underline{\mathbf{W}}}$ respectively) are defined as

$$\overline{\underline{\mathbf{D}}} = (\overline{\underline{\mathbf{L}}} + \overline{\underline{\mathbf{L}}}^{\mathrm{T}})/2, \qquad \overline{\underline{\mathbf{W}}} = (\overline{\underline{\mathbf{L}}} - \overline{\underline{\mathbf{L}}}^{\mathrm{T}})/2. \tag{4}$$

Here, $\overline{\underline{\mathbf{L}}}^{\mathrm{T}}$ designates the transposed tensor of $\overline{\underline{\mathbf{L}}}$.

With the microscopic constitutive relation (3), the crystallographic orientations (i.e., all $\underline{\mathbf{r}}^s$ tensors), and the velocity gradient $\overline{\underline{\mathbf{L}}}$ on the polycrystal scale known, the difficulty of the problem lies in the calculation of a microscopic state ($\underline{\mathbf{s}}$, $\underline{\mathbf{d}}$) for each grain, where its polycrystal volume average (denoted by angle brackets) determines the response of the polycrystal:

$$<\underline{\mathbf{s}}> = \overline{\underline{\mathbf{S}}}, \tag{5}$$

$$<\underline{\mathbf{d}}> = \overline{\underline{\mathbf{D}}}. \tag{6}$$

Then a relation linking microscopic state ($\underline{\mathbf{s}}$, $\underline{\mathbf{d}}$) and macroscopic state ($\overline{\underline{\mathbf{S}}}$, $\overline{\underline{\mathbf{D}}}$) must be introduced. In order to find such a micro-macro relation, which completely determines the response of the polycrystal, some assumptions must be made. In doing this, we use the static, Taylor, and VPSC models.

Within the static approximation, macroscopic and microscopic stress tensors are assumed to be equal:

$$\underline{\mathbf{s}} = \overline{\underline{\mathbf{S}}}. \tag{7}$$

The microscopic strain rate tensor is then given by

$$\underline{\mathbf{d}} = \dot{\gamma}_0 \sum_{s=1}^{S} \underline{\mathbf{r}}^s \left| \frac{\underline{\mathbf{r}}^s:\overline{\underline{\mathbf{S}}}}{\tau_0^s} \right|^{n^s-1} \frac{\underline{\mathbf{r}}^s:\overline{\underline{\mathbf{S}}}}{\tau_0^s}. \tag{8}$$

On the other hand, within the Taylor approximation, a strict uniformity of the velocity gradient is imposed, i.e.,

$$\underline{\mathbf{l}} = \overline{\underline{\mathbf{L}}}, \tag{9}$$

and equation (3) becomes

$$\overline{\underline{\mathbf{D}}} = \dot{\gamma}_0 \sum_{s=1}^{S} \underline{\mathbf{r}}^s \left| \frac{\underline{\mathbf{r}}^s:\underline{\mathbf{s}}}{\tau_0^s} \right|^{n^s-1} \frac{\underline{\mathbf{r}}^s:\underline{\mathbf{s}}}{\tau_0^s}. \tag{10}$$

Both approximations lead to a nonlinear system of equations, which is easily solved with the classical Newton-Raphson iterative method. In this way, the microscopic state ($\underline{\mathbf{s}}$, $\underline{\mathbf{d}}$) can be calculated for any value of the imposed velocity gradient $\overline{\underline{\mathbf{L}}}$.

Within the VPSC approach, the microscopic states differ from the macroscopic state at any location within the polycrystal. In what follows, we present only the main equations in a general way (for further details, see *Lebensohn and Tomé* [1993]). Within this model, the constitutive equation (3) is rewritten in a pseudo-linear form,

$$\underline{\mathbf{d}} = \left\{ \dot{\gamma}_0 \sum_{s=1}^{S} \frac{\underline{\mathbf{r}}^s \otimes \underline{\mathbf{r}}^s}{\tau_0^s} \left| \frac{\underline{\mathbf{r}}^s:\underline{\mathbf{s}}}{\tau_0^s} \right|^{n^s-1} \right\} :\underline{\mathbf{s}} = \underline{\underline{\mathbf{m}}}^{(\mathrm{sec})}(\underline{\mathbf{s}}):\underline{\mathbf{s}}, \tag{11}$$

where $\underline{\underline{\mathbf{m}}}^{(\mathrm{sec})}$ is the secant compliance that gives the instantaneous relation between stress and strain rate. Except when $n^s = 1$ for all systems, $\underline{\underline{\mathbf{m}}}^{(\mathrm{sec})}$ depends on the applied stress, and the validity of relation (11) is limited to the precise point ($\underline{\mathbf{s}}$, $\underline{\mathbf{d}}$) that describes the grain state. This relation can be approximated by a linear form in the vicinity of the stress state $\underline{\mathbf{s}}'$. The tangent compliance $\underline{\underline{\mathbf{m}}}^{(\mathrm{tg})}$ and the back extrapolated term $\underline{\mathbf{d}}^0$ are defined by the first-order Taylor expansion of (3):

$$\underline{\mathbf{d}} = \underline{\underline{\mathbf{m}}}^{(\mathrm{tg})}(\underline{\mathbf{s}}'):\underline{\mathbf{s}} + \underline{\mathbf{d}}^0(\underline{\mathbf{s}}') \tag{12}$$

with

$$m_{ijkl}^{(tg)}(\underline{s}') = \frac{\partial d_{ij}}{\partial s_{kl}}(\underline{s}') . \quad (13)$$

At the macroscopic level, the polycrystal response can be characterized by constitutive equations similar to (12) and (13). It is given by a secant relationship

$$\underline{D} = \underline{\underline{M}}^{(sec)}(\underline{S}):\underline{S} \quad (14)$$

and a tangent relationship in the vicinity of $\overline{\underline{S}}$,

$$\underline{D} = \underline{\underline{M}}^{(tg)}(\overline{\underline{S}}):\underline{S} + \underline{D}^{o}(\overline{\underline{S}}) . \quad (15)$$

Secant and tangent compliance are linked by

$$\underline{\underline{M}}^{(tg)}(\overline{\underline{S}}) = N\underline{\underline{M}}^{(sec)}(\overline{\underline{S}}) \quad (16)$$

where N is the macroscopic stress exponent.

Within the VPSC approach, a homogeneous equivalent medium is considered, whose behavior is identical to that of the whole polycrystal. This HEM is infinite by hypothesis. $\underline{\underline{M}}^{(tg)}$ and $\underline{D}^{o}$ are taken as frozen to the values $\underline{\underline{M}}^{(tg)}(\overline{\underline{S}})$ and $\underline{D}^{o}(\overline{\underline{S}})$ in the HEM. Thus $\underline{L}$, $\underline{D}$ and $\underline{S}$ define velocity gradient, deformation rate, and deviatoric stress inside the HEM, at a given location. $\overline{\underline{L}}$, $\overline{\underline{D}}$, and $\overline{\underline{S}}$ correspond to the same quantities infinitely far from this location.

As a simplification, the so-called "one-site" approximation is used within the formulation of *Lebensohn and Tomé* [1993]. The calculation of stress and deformation rate of a grain does not take into account the influence of neighboring grains. However, a significant influence of neighboring grains has been observed in experimentally deformed dolomite [*Barber et al.*, 1994] and ice [*Azuma*, 1995]. This one-site approximation does not then permit the evaluation of vicinity effects but should remain valid for average predictions. Thus each grain is considered successively as an inclusion in the HEM, whose behavior is given by equation (15), and submitted to the uniform velocity gradient $\overline{\underline{L}}$ at infinity. This interaction problem is solved using the inclusion problem formalism [*Eshelby*, 1957; *Hill*, 1965]. Since grain shape is assumed to be ellipsoidal and the HEM to have a linear (tangent) behavior, a uniform strain rate $\underline{d}$ and uniform stress $\underline{s}$ develop in each grain. Therefore the microscopic constitutive equation (12) can be rewritten

$$\underline{d} = \underline{\underline{m}}^{(tg)}(\underline{s}):\underline{s} + \underline{d}^{o}(\underline{s}) . \quad (17)$$

The Eshelby solution of the viscoplastic inclusion problem leads to the interaction equation

$$\underline{d} - \overline{\underline{D}} = -\underline{\underline{\tilde{M}}}:(\underline{s} - \overline{\underline{S}}) , \quad (18)$$

where the interaction tensor $\underline{\underline{\tilde{M}}}$ is defined as

$$\underline{\underline{\tilde{M}}} = (\underline{\underline{I}} - \underline{\underline{S}}^{Esh})^{-1}:\underline{\underline{S}}^{Esh}:\underline{\underline{M}}^{(tg)} \quad (19)$$

In (19), $\underline{\underline{I}}$ is the fourth-rank identity tensor for symmetrical tensors, and $\underline{\underline{S}}^{Esh}$ is the viscoplastic Eshelby tensor [*Lebensohn and Tomé*, 1993], a function of the tangent viscoplastic compliance $\underline{\underline{M}}^{(tg)}$ and of the shape of the inclusion. In addition, the behavior of grains appears in (18) only implicitly via the constitutive equation (11) relating $\underline{s}$ and $\underline{d}$. However, the viscoplastic compliance is not known in advance. Therefore a self-consistent expression from which $\underline{\underline{M}}^{(sec)}$ can be calculated must be found. Condition (6) is rewritten, together with the secant relations (11) and (14) and the interaction equation (18):

$$\underline{\underline{M}}^{(sec)} = <\underline{\underline{m}}^{(sec)}:\underline{\underline{B}}> \quad (20)$$

where the accommodation tensor $\underline{\underline{B}}$ is defined as

$$\underline{\underline{B}}:\overline{\underline{S}} = \underline{s} . \quad (21)$$

Concerning the first-order Taylor development of the macroscopic constitutive relation, it is important to note that (15) is exact only when it describes the strain rate associated to the stress $\overline{\underline{S}}$ used as reference for the expansion, or when (14) is linear (i.e., for N=1). Otherwise, it is only approximate. A limitation of the tangent formulation appears then when (15) is used to estimate the response of the HEM in the vicinity of the inclusion, where local variation of strain rate and stress takes place. This variation has to be within the interval where the tangent approximation is assumed to be adequate. However, at a given value of the stress deviation $\underline{S} - \overline{\underline{S}}$ near the inclusion, the error in the value of the strain rate calculated with the tangent approximation (15) increases exponentially with the stress exponent N. The application of the VPSC model to zirconium alloy [*Lebensohn and Tomé*, 1993] shows that the tangent approximation is valid for values of N smaller than 20. The anisotropy of ice crystals is very large, but the stress exponent of polycrystalline ice is close to 1 ($1 \le N \le 3$). Thus the tangent approximation must also be valid in our case.

Within the formulation of this VPSC model, the interaction tensor $\underline{\underline{M}}$ and the macroscopic compliance $\underline{\underline{M}}^{(tg)}$ are fully determined. This allows this HEM to have any anisotropic response.

Once convergence is achieved, the rotation rate $\underline{w}^{c}$ of crystallographic axes, which determines the fabric evolution, is calculated for each grain. It is expressed for the VPSC model as

$$\underline{w}^{c} = \overline{\underline{W}} + \underline{w}^{e} - \underline{w}^{p} . \quad (22)$$

The rotation rate $\underline{w}^{e}$ of the associated ellipsoid and the plastic rotation rate $\underline{w}^{p}$ are given respectively by

$$\underline{w}^{e} = \underline{\underline{\Pi}}^{Esh}:\underline{\underline{S}}^{Esh^{-1}}:(\underline{d} - \overline{\underline{D}}) \quad (23)$$

$$\underline{w}^{p} = \sum_{s=1}^{S} \frac{1}{2}(\mathbf{n}^{s} \otimes \mathbf{b}^{s} - \mathbf{b}^{s} \otimes \mathbf{n}^{s})\dot{\gamma}^{s} , \quad (24)$$

where $\underline{\underline{\Pi}}^{Esh}$ denotes the skew-symmetric Eshelby rotation tensor [*Lebensohn and Tomé*, 1993]. The influence of the term $\underline{w}^{e}$ increases with the anisotropy of the HEM and with the distortion of the grain shape. Within the Taylor approximation, $\underline{w}^{e}$ vanishes, and $\underline{w}^{c}$ is given by

$$\underline{w}^{c} = \overline{\underline{W}} - \underline{w}^{p} . \quad (25)$$

This latter relation (25) is also used for the static model. This implies implicitly that the local rotation rate is equal to the macroscopic rotation rate $\overline{\underline{W}}$. Thus the static model is incoherent in the way in which a compatibility condition is imposed on the rotation, but not on the deformation.

In this paper, we use Von Mises equivalent deviatoric stress $\bar{S}_{eq}$ and strain rate $\bar{D}_{eq}$ as an average measure of the deviatoric stress and strain rate:

$$\bar{S}_{eq} = \sqrt{\frac{3}{2}\underline{\bar{S}}:\underline{\bar{S}}}\,, \qquad \bar{D}_{eq} = \sqrt{\frac{2}{3}\underline{\bar{D}}:\underline{\bar{D}}}\,. \tag{26}$$

Deformations are computed in extension, compression, and simple shear. The imposed velocity gradients are constant. They are given respectively by (in units of reciprocal seconds)

$$\underline{\bar{L}} = \begin{bmatrix} 1.0 & 0 & 0 \\ 0 & -0.5 & 0 \\ 0 & 0 & -0.5 \end{bmatrix} \tag{27}$$

$$\underline{\bar{L}} = \begin{bmatrix} 0.5 & 0 & 0 \\ 0 & 0.5 & 0 \\ 0 & 0 & -1.0 \end{bmatrix} \tag{28}$$

$$\underline{\bar{L}} = \begin{bmatrix} 0 & 0 & \sqrt{3} \\ 0 & 0 & 0 \\ 0 & 0 & 0 \end{bmatrix} \tag{29}$$

so that $\bar{D}_{eq}$=1.0 s^{-1} for each deformation case.

Large imposed deformations are decomposed into a sum of small deformation steps (increments), during which all quantities are assumed to remain constant. Time step dt^k is chosen so that each deformation step k leads to a 1% equivalent strain for the polycrystal:

$$\bar{\varepsilon}^k_{eq} = \bar{D}^k_{eq}.dt^k = \frac{1}{100}\,. \tag{30}$$

The total (cumulative) equivalent deformation is the sum over all K deformation steps

$$\bar{\varepsilon}_{eq} = \sum_{k=1}^{K} \bar{\varepsilon}^k_{eq} = \frac{K}{100} \tag{31}$$

and represents only a measure of the deformation. The transformation gradient tensor $\underline{\bar{F}}^k$ for the polycrystal corresponding to the deformation step k is given by

$$\underline{\bar{F}}^k = \exp(dt^k.\underline{\bar{L}})\,, \tag{32}$$

where the exponential function is defined, for second-order tensors, by the relation

$$\exp(\underline{A}) = \underline{I} + \underline{A} + \frac{\underline{A}^2}{2!} + \ldots + \frac{\underline{A}^n}{n!} + \ldots\,. \tag{33}$$

The total transformation gradient tensor $\underline{\bar{F}}$ is calculated with

$$\underline{\bar{F}} = \underline{\bar{F}}^k.\underline{\bar{F}}^o\,, \tag{34}$$

where $\underline{\bar{F}}^o$ is the total transformation gradient of the polycrystal at step k-1. Therefore when velocity gradient and time step are constant, $\underline{\bar{F}}$ is linked to $\bar{\varepsilon}_{eq}$ by the relation

$$\underline{\bar{F}} = \exp\left(\frac{\bar{\varepsilon}_{eq}}{\bar{D}_{eq}}\underline{\bar{L}}\right). \tag{35}$$

Within the following applications, polycrystals are made up of 200 grains, and the value of the reference strain rate $\dot{\gamma}_0$ is taken to be unity (1.0 s^{-1}). Since five independent slip systems can be needed, the ice crystal is supposed to deform by dislocation glide on basal, prismatic and pyramidal planes. Slip systems are summarized in Table 1. The pyramidal system is that proposed by *Hutchinson* [1977] and *Duval et al.* [1983]. Taking the unit vector $\mathbf{e}_3$ of the reference frame parallel to the c axis of the crystal, dislocation motion on basal planes gives the deformations ε_{13} and ε_{23}, on prismatic planes ε_{11}, ε_{22}, and ε_{12}, and on pyramidal planes ε_{11}, ε_{22}, ε_{33}, ε_{23}, ε_{13}, and ε_{12}. Thus basal and prismatic slips produce only distinct deformations. If pyramidal slip is omitted, axial deformation along the c axis is impossible.

Before deformation, grains are supposed equiaxed (spherical shape). As deformation proceeds, grain shape is updated with respect to the macroscopic (average) velocity gradient. Thus all grains exhibit the same shape, regardless of their individual deformation.

Modeling Behavior of Isotropic Polycrystalline Ice

Within all the models described previously, the RRSS of each slip system is the only tuning parameter. The aim of this section is to estimate the RRSS of basal, prismatic, and pyramidal systems, in order to reproduce the behavior of the isotropic polycrystalline ice determined experimentally.

The creep behavior of an isotropic ice polycrystal is well described by the Norton-Hoff constitutive law [*Duval*, 1976], usually used in glaciology:

$$\bar{D}_{ij} = \frac{B_0}{2}\tau^{N-1}\bar{S}_{ij} \tag{36}$$

where B_0 is a scalar, and where the effective shear stress τ is defined as

$$\tau^2 = \frac{1}{2}\underline{\bar{S}}:\underline{\bar{S}} = \frac{1}{3}\bar{S}^2_{eq}\,. \tag{37}$$

This law can be rewritten, without a loss of generality, as a function of Von Mises equivalent stress and strain rate [*Hutchinson*, 1976]:

$$\bar{D}_{ij} = \frac{3}{2}\frac{\bar{D}_{eq}}{\bar{S}_{eq}}\bar{S}_{ij} \tag{38}$$

Table 1. Slip Systems, Total Number of Systems in Each Family, Strains Given by Dislocation Motion, Stress Exponent n^s, and Reference Resolved Shear Stress

	Slip Systems	Number of Systems	Resulting Deformation	n^s	RRSS
Basal	{0001}<11$\bar{2}$0>	3	ε_{13}, ε_{23}	3	τ_a
Prismatic	{01$\bar{1}$0}<2$\bar{1}\bar{1}$0>	3	ε_{11}, ε_{22}, ε_{12}	3	τ_b
Pyramidal	{11$\bar{2}$2}<11$\bar{2}\bar{3}$>	6	ε_{11}, ε_{22}, ε_{33}, ε_{23}, ε_{13}, ε_{12}	3	τ_c

with

$$\overline{D}_{eq} = \dot{\gamma}_o \left(\frac{\overline{S}_{eq}}{\sigma_o} \right)^N . \quad (39)$$

For a complete equivalence of both expressions, a relation linking the macroscopic reference equivalent stress σ_o with B_o must be added:

$$B_o = \dot{\gamma}_o \frac{\sqrt{3}^{N+1}}{\sigma_o{}^N} . \quad (40)$$

We restrict this study to the stress domain where the value of the stress exponent for polycrystalline ice is N=3 (i.e., for $\overline{S}_{eq} > 0.2$ MPa). In this domain the flow law coefficient B_o and the reference stress σ_o can be determined from creep data (Figure 2). At -10°C:

$$B_o = 1.1 \times 10^{-6}\,\mathrm{MPa}^{-3}\,\mathrm{s}^{-1} \quad \sigma_o = 200\,\mathrm{MPa} . \quad (41)$$

Owing to the dispersion of experimental points, the value of σ_o is precise at about ±30%.

Now let τ_a, τ_b, and τ_c denote the RRSS of basal, prismatic, and pyramidal slip systems respectively (Table 1). Basal plane presents three glide directions, each of them forming a 120° angle with respect to the others. From equation (3), the plastic anisotropy on the basal plane can be assumed, except for n^{basal}=1 or n^{basal}=3. But this anisotropy is very weak for $1 < n^{basal} < 4$, and the deviation between the direction of the applied shear stress on the basal plane and the glide direction does not exceed 2.9° [*Kamb*, 1961]. When a monocrystal is sheared on the basal plane so that the direction of the shear stress is aligned exactly in the direction of an *a* axis, equation (3) can be rewritten as the following expression, when only basal slip is taken into account:

$$d_{eq}^{basal} = \dot{\gamma}_o \frac{1}{\sqrt{3}^{n^{basal}+1}} \left(1 + \frac{1}{2^{n^{basal}}} \right) \left(\frac{s_{eq}^{basal}}{\tau_a} \right)^{n^{basal}} . \quad (42)$$

The stress exponent N of the polycrystal depends on the rate sensitivity of each slip system. The value n^{basal}=2 has been found experimentally for an isolated single crystal. Since a grain boundary cannot produce (and absorb) dislocations in a similar way to a free surface, a different value of n^{basal} is expected for a grain embedded within a polycrystal. In this study we take n^s=3 for each system. As a result, we get N=3. The top curve of Figure 2 together with (42) gives, for s_{eq}^{basal}=1 MPa and n^{basal}=3,

$$\tau_a = 11\,\mathrm{MPa} . \quad (43)$$

Similarly, from data on the nonbasal creep behavior of monocrystals, lower bounds for τ_b and τ_c can be obtained:

$$\tau_b \geq 27\tau_a , \qquad \tau_c \geq 39\tau_a . \quad (44)$$

We get then, from relations (41) and (43),

$$\sigma_o/\tau_a = 18 . \quad (45)$$

For a given strain rate, σ_o / τ_a expresses the ratio between the viscosity of isotropic ice and the viscosity of a single crystal deformed by basal glide. Note that this value of 18 was obtained from mechanical tests only and is therefore entirely independent of polycrystal models.

Let us now compare the results given above, resulting from mechanical tests, with those obtained from static, Taylor, and VPSC approximations. Figure 3a shows the evolution of σ_o / τ_a against values of the RRSS of nonbasal systems relative to τ_a, when the resistance for prismatic and pyramidal systems are equal ($\tau_b = \tau_c$). The deviation between polycrystal models becomes large with low values of τ_a / τ_b. When dislocation glide is entirely suppressed on prismatic and pyramidal planes, i.e., for $\tau_b = \tau_c = \infty$, the upper bound estimate of σ_o / τ_a is unbounded; overall deformation cannot occur when slip takes place only on basal planes. On the other hand, the maximal values obtained with the VPSC and the lower bound estimates are σ_o / τ_a=33 and σ_o / τ_a=3.2 respectively. This latter value is too low compared with that given in (45). Thus the static model cannot describe the behavior of polycrystalline ice.

From Figure 3b the corresponding relative activity of basal systems, defined as the relative contribution of basal slip to the total (macroscopic) deformation, increases with decreasing values of τ_a / τ_b. When $\tau_b = \tau_c > 10\tau_a$, basal slip contributes more than 99% to the total deformation with

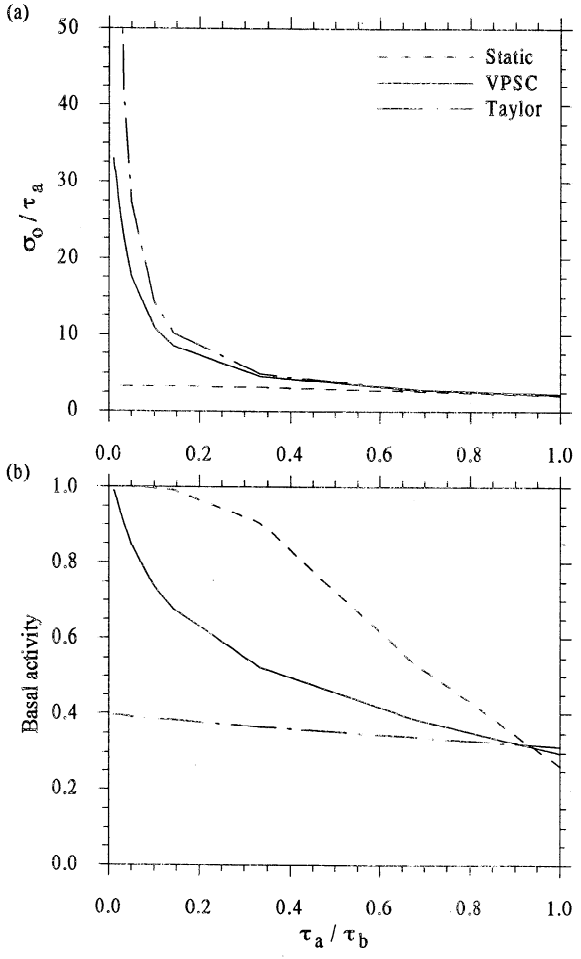

Figure 3. Response of a randomly oriented polycrystal (isotropic), as a function of the relative hardness τ_a / τ_b of prismatic and pyramidal glide systems, with $\tau_b = \tau_c$. (a) Ratio between reference stresses, σ_o / τ_a. (b) Relative activity of basal slip.

the lower bound and more than 70% with the VSPC approach.

With the VPSC approximation, stress and deformation states are not homogeneous within the polycrystal. This model gives an intermediate solution, between that of the lower and upper bound, for both the activity of basal systems and the polycrystal rheology. As with the Taylor model, the viscosity of an isotropic polycrystal becomes large when both prismatic and pyramidal slips are suppressed. The evolution of basal activity against τ_a / τ_b is, however, quite close to that given by the static model. For $\tau_b = \tau_c > 100\,\tau_a$, basal slip contributes more than 99% to the total deformation, but the viscosity of the polycrystal remains controlled by the large RRSS of nonbasal systems.

Both VPSC and Taylor models are able to reproduce the viscosity of isotropic polycrystalline ice. The experimental value $\sigma_0 / \tau_a = 18$ is found with $\tau_b = \tau_c = 20\,\tau_a$ for the VPSC model and $\tau_b = \tau_c = 12\,\tau_a$ for the Taylor model (Figure 3a). From the experimental values given in (44), the VSPC model seems to be more suitable than the Taylor approach. This is confirmed by results on the activity of basal systems given in Figure 3b. Indeed, the Taylor model predicts that about 60% of the total deformation is due to dislocation glide on nonbasal systems. This estimation is not realistic,

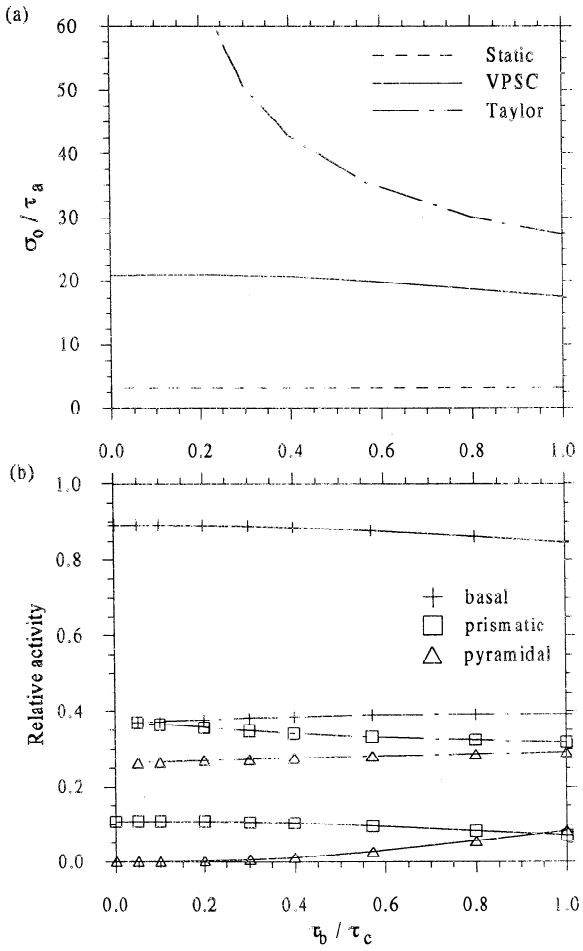

Figure 4. Response of a randomly oriented polycrystal (isotropic), as a function of the relative hardness τ_b / τ_c of the pyramidal systems, with $\tau_b = 20\,\tau_a$. (a) Ratio between reference stresses, σ_0 / τ_a. (b) Relative activity of slip systems for Taylor and VPSC models.

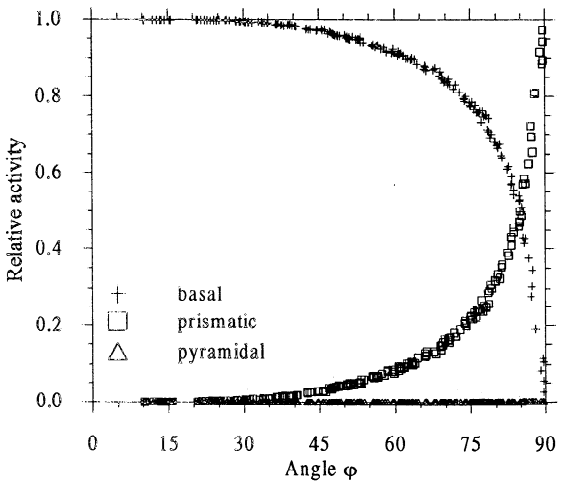

Figure 5. Relative activity of basal, prismatic, and pyramidal slip systems in each grain of a randomly oriented polycrystal deformed in uniaxial compression. Here, φ is the angle between the *c* axis and the direction of uniaxial compression. Results of the VPSC model.

since the major part of dislocations observed in ice crystals lies in the basal planes [*Higashi et al.*, 1985; *Ahmad and Whitworth*, 1988].

Figure 4 shows the response of an isotropic polycrystal, but now with $\tau_b = 20\,\tau_a$, and for increasing values of the RRSS of pyramidal slip systems relative to the value of the prismatic RRSS. The limit $\tau_c = \infty$ corresponds to the case where only basal and prismatic slip are allowed. In that case the predicted viscosity is infinite with the upper bound. The basal system never contributes more than 40% to the total deformation (Figure 4b). A different behavior is found with the VPSC model. The ratio σ_0 / τ_a does not significantly change with τ_b / τ_c and is close to the experimental value. The resistance ratio between prismatic and basal systems is therefore close to 20, i.e., a value compatible with creep data on monocrystals (equation (44)). Therefore calculations based on the VSPC method show that the viscoplasticity of polycrystalline ice can be described by invoking only basal and prismatic slip. Overall compatibility is possible without axial deformation along the *c* axis, since only pyramidal slip can produce such a deformation. From Figure 4b the activity of prismatic systems is not more than 10%. However, this system fully controls the viscosity of the polycrystal.

Now, we will take for all the following calculations

$$\tau_a = \frac{\tau_b}{20} = \frac{\tau_c}{200} \tag{46}$$

so that the self-consistent model exactly reproduces the behavior of an isotropic polycrystal and so that pyramidal slip is minimized. Macroscopic reference axial stresses σ_0 are given by

$$\tau_a = \frac{\sigma_0^{\text{static}}}{3.2} = \frac{\sigma_0^{\text{VPSC}}}{20.5} = \frac{\sigma_0^{\text{Taylor}}}{117} \; . \tag{47}$$

In order to determine the state of each grain, a uniaxial deformation test was performed on an isotropic polycrystal. In Figure 5 we have plotted the relative activities found with the self-consistent theory against the angle φ between each *c* axis and the direction of uniaxial deformation. It appears that

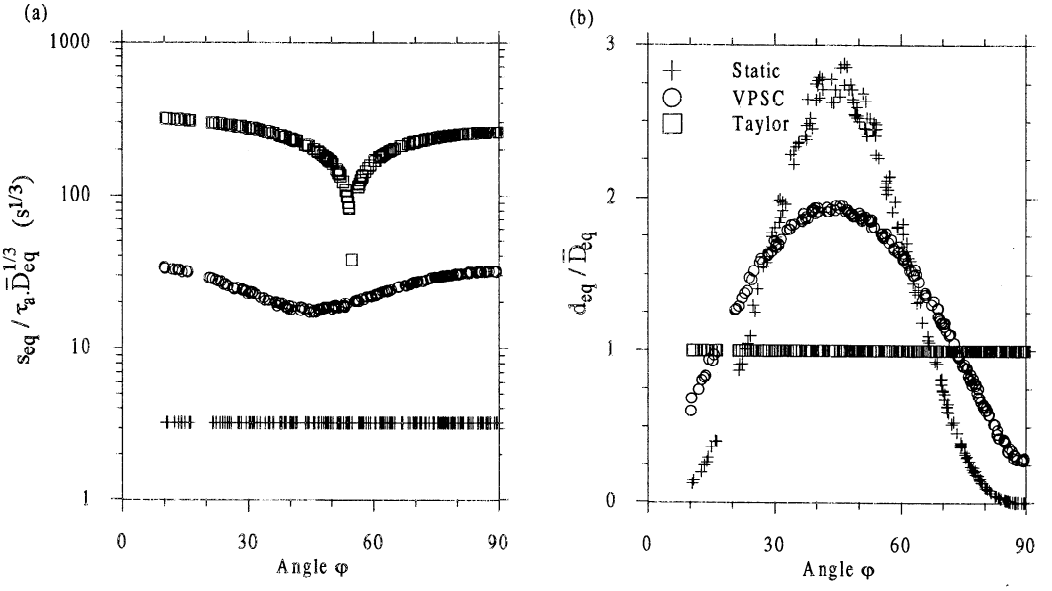

Figure 6. (a) Normalized equivalent stress and (b) normalized equivalent strain rate in each grain of an isotropic polycrystal deformed in uniaxial compression. Here, φ is the angle between the *c* axis and the direction of uniaxial compression. Results of the VPSC model.

the deformation of grains corresponding to $5° < \varphi < 50°$ is possible with less than 5% activity of nonbasal systems. For larger values of φ a significant activation of prismatic systems is necessary, but overall compatibility is possible without pyramidal slip. The activity of pyramidal systems is larger than 1% only for $\varphi \leq 5°$. A maximal value of 15% is found for $\varphi = 0°$, i.e., when the *c* axes are precisely aligned with the direction of uniaxial deformation. Similarly, Figure 6 gives normalized equivalent stress and strain rate in each grain, predicted by static, VPSC, and Taylor models. The lower bound gives a maximum strain rate at $\varphi = 45°$. The stress obtained with the Taylor model is found at its minimum at about 55°. The self-consistent theory predicts an intermediate behavior, with a minimum stress and a maximum strain rate at $\varphi = 45°$. Note that the large strain rate deviation obtained with this model is comparable to that obtained with the static model.

In the previous section, static, VPSC, and Taylor models are described separately. However, a direct comparison is possible when an interaction coefficient α is introduced in (18):

$$\underline{\mathbf{d}} - \overline{\underline{\mathbf{D}}} = -\alpha \underline{\underline{\tilde{\mathbf{M}}}} : (\underline{\mathbf{s}} - \overline{\underline{\mathbf{S}}}) \qquad (48)$$

where α is a positive scalar quantity. This term expresses the interaction stiffness between grain and matrix. For polar ice it could represent the accomodation processes, i.e., the effects of grain boundary migration. Of course, $\alpha = 1$ leads to the VPSC estimation. The theoretical limit $\alpha = \infty$ corresponds to the static model (infinitely soft interaction), and $\alpha = 0$ correponds to the Taylor model (infinitely hard interaction). Numerically, a difference of less than 1% between values of σ_0 / τ_a calculated with real static and Taylor models (i.e., equations (8) and (10)) and values calculated with (48), is found for $\alpha \geq 100$ and $\alpha \leq 0.01$, respectively (Figure 7). Thus both static and Taylor approximations can be considered as extreme solutions of the viscoplastic inclusion problem. Since (48) is the only relation linking microscopic and macroscopic states within the VPSC model, a continuous variation of the polycrystal response, from uniform strain to uniform stress, is found by tuning this interaction coefficient α. From Figure 7, the sensitivity to α of the polycrystal response σ_0 / τ_a is the largest for the self-consistent estimate.

Fabric Development

Simulation

Figure 8 displays *c* axis fabric diagrams obtained in uniaxial extension, uniaxial compression, and simple shear, after 0.4 equivalent strain, and where the initial polycrystal was randomly oriented (i.e., isotropic). Since the self-consistent model permits us to account for variations in the grain shape with strain, simulations were performed both with and without evolution of the grain shape, i.e., with an

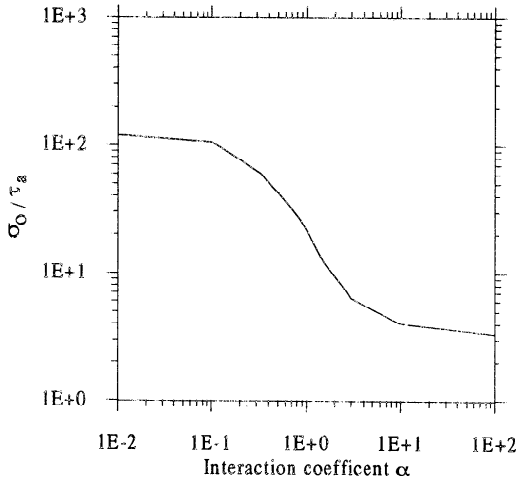

Figure 7. Influence of the interaction coefficient α on the strengh of an isotropic polycrystal.

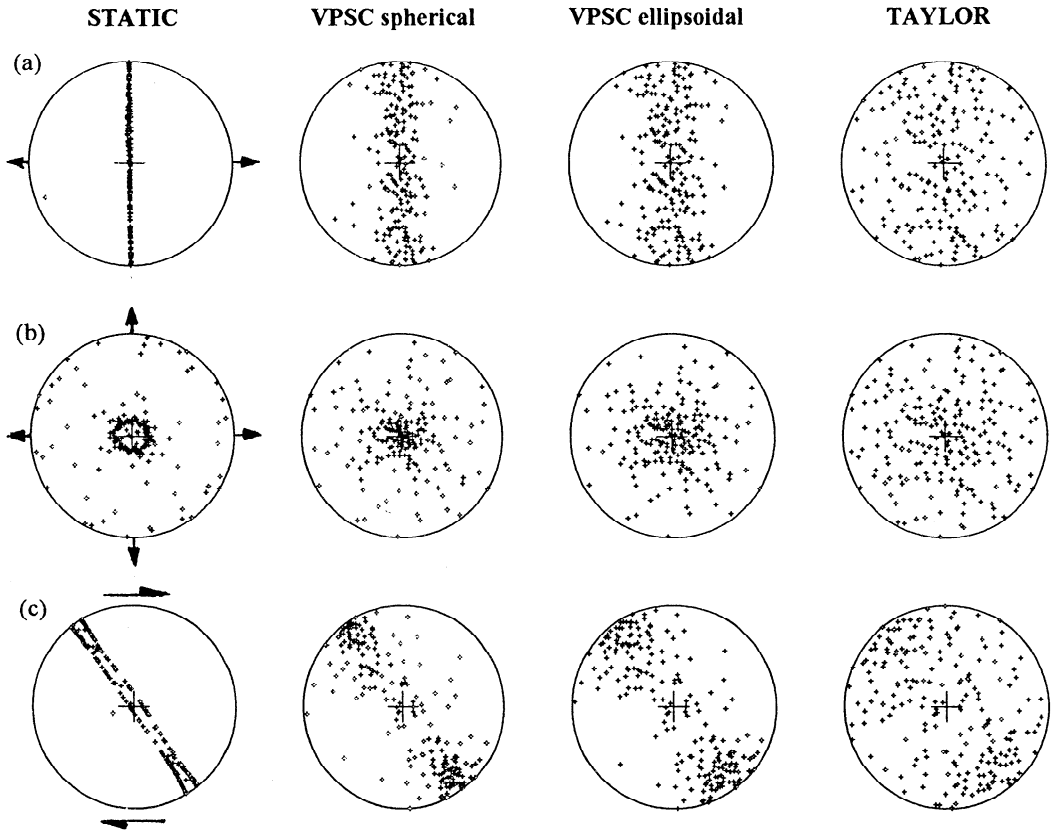

Figure 8. Diagrams of c axis fabric simulated with the static, VPSC (constant spherical grain shape and evolutive ellipsoidal grain shape), and Taylor models: (a) Uniaxial extension. (b) Uniaxial compression. (c) Simple shear. Here, $\varepsilon_{eq} = 0.4$. The initial polycrystal was randomly oriented. Equal-area projection. Arrows denote the direction of deformation.

evolutive ellipsoidal and a constant spherical grain shape (denoted VPSC ellipsoidal and VPSC spherical, respectively).

Qualitatively, all models predict the same fabric pattern. In uniaxial extension we found a concentration of c axes around the plane normal to the direction of extension. In uniaxial compression a single maximum fabric develops, where c axes rotate toward the direction of maximal compression. Nevertheless, in simple shear we found a single maximum fabric, but this maximum lies between the normal to the macroscopic shear plane and the principal direction of compression.

Large differences between all models appear in the preferential orientation of c axes for the same equivalent strain of 0.4. We get extremely concentrated fabrics with the static model and very slightly pronounced ones with the Taylor model. Predictions from the VPSC model lie between the two of them but depend on the evolution of grain shape. Fabrics obtained with evolutive grain shape are less concentrated than those obtained with constant spherical shape.

Orientation changes are directly linked to slip system activity. In Figure 9 we have plotted the number of active slip systems against equivalent strain. In viscoplastic deformation modeling, mathematically all systems are active, but some contribute only a very small amount to the total strain.

In each grain we consider a slip system as active if its contribution to the total shear of the grain is more than 5% of that of the most active system. The average number of slip systems is calculated for the whole polycrystal, where the number of active systems in each grain is weighted by the total shear of this grain.

In uniaxial extension and compression, stable values around 2.3 and 9.5 are found with static and Taylor models, respectively. Results from the VPSC model present much larger variations, especially in compression with spherical grains, where a maximal value of about 7 is found for a strain between 0.7 and 0.8. In extension, no more than four systems are activated, and we get decreasing values after 0.5 equivalent strain. Generally speaking, the number of active systems is more constant with distorted grain shapes.

A more detailed analysis can be made by considering the relative activity of all slip systems, as shown in Figure 10. Diagrams for the static model have not been plotted, since the relative contribution of nonbasal systems always represents less than 1%.

In extension, results obtained with the self-consistent model with and without grain shape change are qualitatively similar. The basal slip activity is decreasing continually and is progressively replaced by prismatic slip. In compression with spherical grains, basal activity presents first a quasi-steady stage, during which the fabric becomes very concentrated, as is shown in Figure 8. Afterward, basal slip decreases and is replaced by pyramidal slip, which attains considerable activity. With evolutive grain shape, basal slip retains a very large activity, and pyramidal slip is activated only after an equivalent strain of 0.8. Nevertheless, the same kinds of

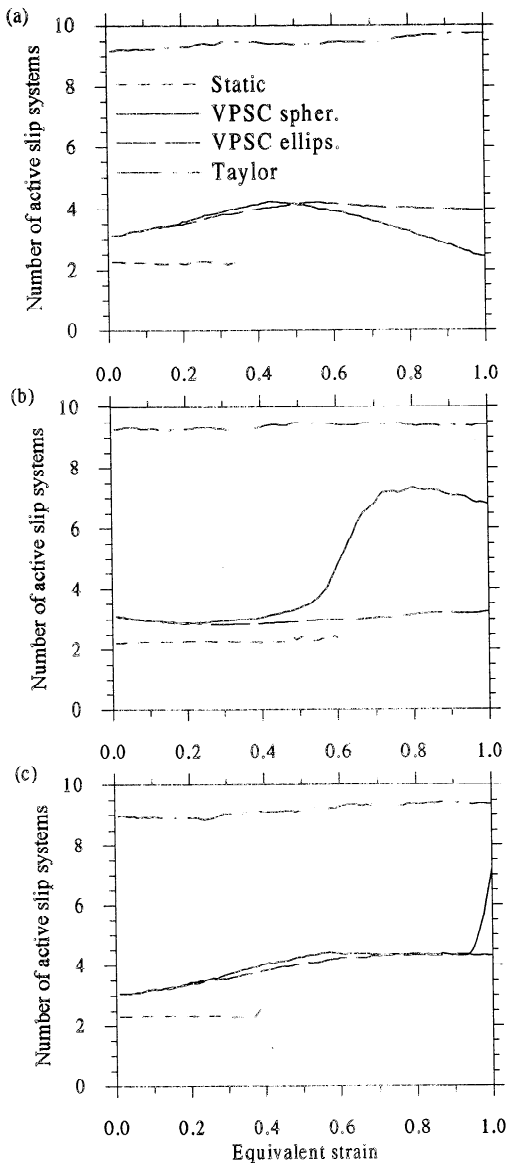

Figure 9. Number of active slip systems versus equivalent strain, for deformations in (a) uniaxial extension, (b) uniaxial compression, and (c) simple shear. The initial polycrystal was randomly oriented. Results of the static model have not been plotted for strain larger than 0.4 and 0.6, since extremely prononced textures appear.

fabrics are observed for uniaxial extension and compression, with c axes aligned toward the principal direction(s) of compression.

As was discussed in the previous section, a uniform strain rate field in the polycrystal can be reached only with an extensive activity of nonbasal systems. Therefore since the activity predicted with the Taylor model presents an evolution similar to that of the VPSC model, variations are smoother, and no system really predominates for strain as large as 1.0. Note that an increasing nonbasal activity slows down the rotation rate of c axes, but does not influence the character of final fabrics. Indeed, even with a large activity of nonbasal systems (as obtained with Taylor and VPSC models), patterns of final fabrics are similar to those found with the static model, where only basal systems are activated.

In simple shear, two mechanisms are in competition for fabric development: rotation of the c axes toward the principal direction of compression, and dragging of the fabric maximum by the macroscopic rotation. Fabrics obtained with VPSC and Taylor models for an equivalent strain of 0.4 (Figure 8) are not stable: the maximum continues to turn slowly toward the normal to the macroscopic shear plane as deformation proceeds (Figure 11). At an equivalent strain of 5, the deviation between this normal orientation and the fabric maximum is about 5°. However, a stable fabric is reached with the lower bound at an equivalent strain of only 0.5. With this model, a much larger deviation (30°) is obtained.

At 0.4 equivalent strain, most grains are oriented for hard glide deformation. With the self-consistent approach, prismatic systems are significantly activated. At this stage, the deformation is possible without axial deformation along the c axis (Figures 9 and 10). Pyramidal slip occurs only for larger deformation. On the other hand, results from the upper bound show quasi constant activities for each system, which are all about 30%. With the static model, only basal systems are activated, and basal planes are inclined to the macroscopic shear plane, against the sense of shear. Thus it appears that a significant activation of nonbasal systems is necessary for the rotation of the fabric maximum. Under these conditions, c axes turn away from the principal direction of compression and toward the normal to the macroscopic shear plane. The macroscopic rotation rate $\underline{\overline{W}}$ predominates until this stable position is reached.

Comparison With Fabrics in Polar Ice Sheets

Fabric formation in ice sheets is interpreted by the rotation of crystallographic axes by slip as long as the nucleation of grains and grain boundary migration are not significant. At first approximation, this is the case in zones in which grain growth or rotation recrystallization occurs.

Simulated fabrics are compared with fabrics along three deep ice cores in Antarctica: Vostok at 915 m depth [*Lipenkov et al.*, 1989], Dome C at 850 m depth, and Byrd at 1570 m depth [*Gow and Williamson*, 1976]. Fabric patterns are shown in Figure 12. In these diagrams the in situ vertical direction corresponds to the center of the circle. Vostok and Dome C samples are still within the grain growth zone. At Byrd, grain growth stops at a depth of about 400 m, while polygonization associated with rotation recrystallization occurs until 1800 m [*Alley et al.*, 1995].

According to *Lipenkov et al.* [1989], ice at Vostok Station above a depth of 2083 m is deformed by horizontal extension. The surface slope being smaller than 10^{-3}, the horizontal shear stress is not significant above this depth. The total deformation of the Vostok ices can be estimated assuming a uniform vertical strain rate along the core and a steady state for the flow. Assuming an accumulation rate corresponding to that of the last glacial period, we find that the equivalent strain at 915 m should be around 0.4. The kinetics of fabric development obtained with the self-consistent scheme compares well with this estimation (Figure 8).

At Dome C, ice is deformed by vertical compression. In Figure 12b, c axes are clearly concentrated around the vertical direction. An equivalent strain of about 0.2 is found at a depth of 850 m. In order to quantify the strengthening of fabrics, we introduce the half apex angle θ of a cone whose

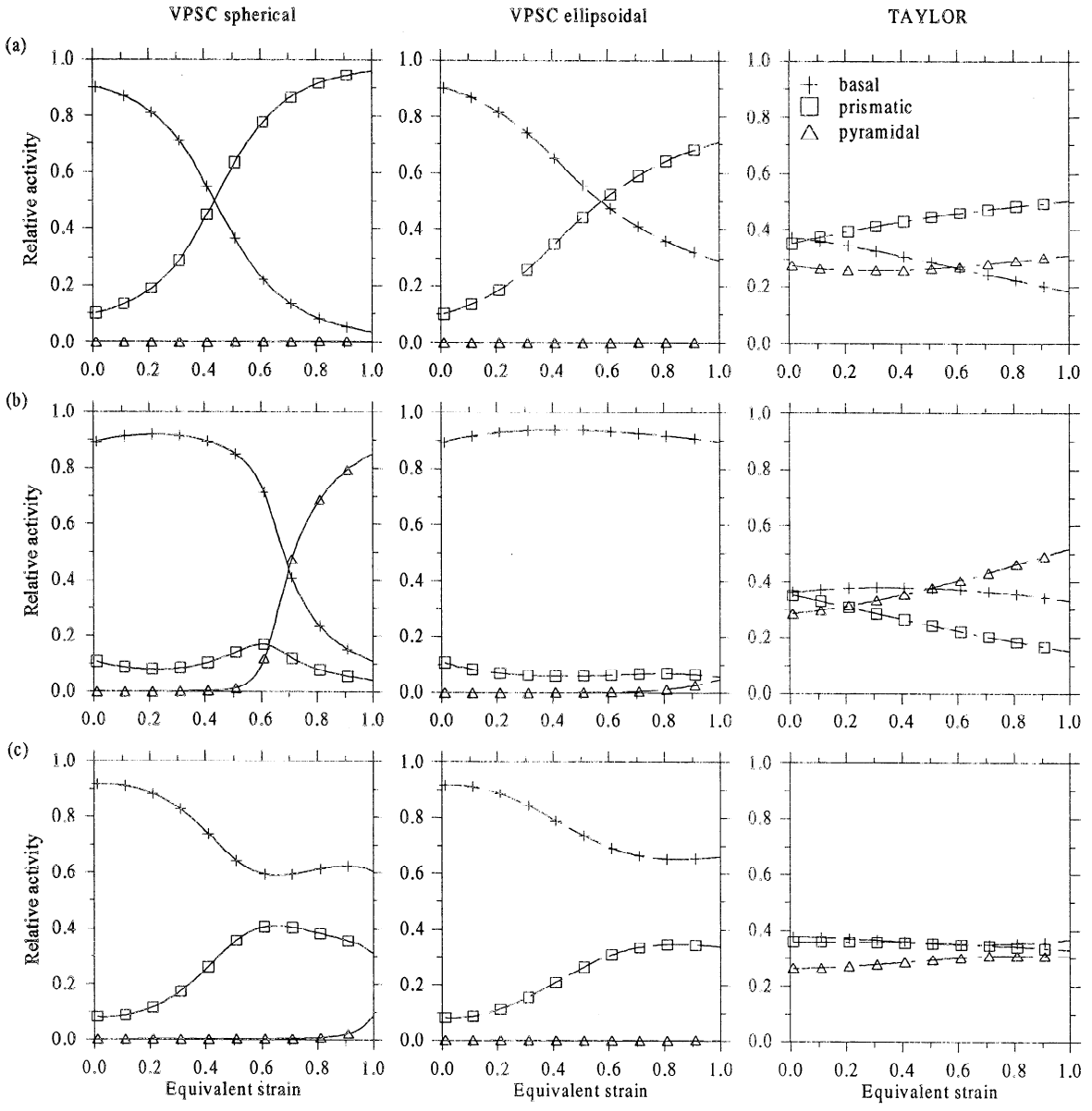

Figure 10. Relative activity of basal, prismatic, and pyramidal slip systems from VPSC (with and without grain shape evolution) and Taylor models: (a) uniaxial extension, (b) uniaxial compression, and (c) simple shear. The initial polycrystal was randomly oriented. Within the static model (not reported here), nonbasal activity is always lower than 1%.

revolution axis coincides with the symmetry axis of fabrics and that contains 50% of *c* axes. The angle $\theta = 60°$ then corresponds to an isotropic polycrystal. The half apex angle θ of this Dome C fabric is 42°. Static, VPSC, and Taylor models predict a fabric similarly concentrated for an equivalent strain of 0.15, 0.2, and 0.45, respectively. In that case, only the upper bound can be disregarded. It seems then that the fabric evolution rate calculated with the lower bound is too rapid for uniaxial deformation. On the other hand, the upper bound seems to underestimate the *c* axes' rotation rate. The best fit would be obtained with the self-consistent theory, but for this low accumulated strain, such a result should be considered carefully.

At Byrd Station, the vertical compression strain rate is close to $2\times10^{-12}s^{-1}$, but because of the relatively important surface slope (around 3×10^{-3}), the horizontal shear strain rate should exceed $5\times10^{-11}s^{-1}$ below a depth of 400 m [*Lliboutry and Duval*, 1985]. Therefore simple shear can be assumed to dominate along the 2164 m ice core. Only a lower bound for the accumulated strain can be obtained at a depth of 1570 m. With a mean value of the shear strain rate of $5\times10^{-11}s^{-1}$, the equivalent strain is higher than 10. The fabric shown in Figure 12c for this depth shows that most *c* axes have a nearly vertical orientation. This fabric is consistent with that obtained with the VPSC and the Taylor models for strain larger than 5. However, the intermediate fabrics obtained with these models, at an equivalent strain of 0.4 (Figure 8), have never been observed in deep ice cores.

An attempt to simulate fabric evolution with a more realistic in situ deformation history is presented in Figure 13. With the VPSC model, we have imposed on an isotropic polycrystal first a vertical compression and then a simple

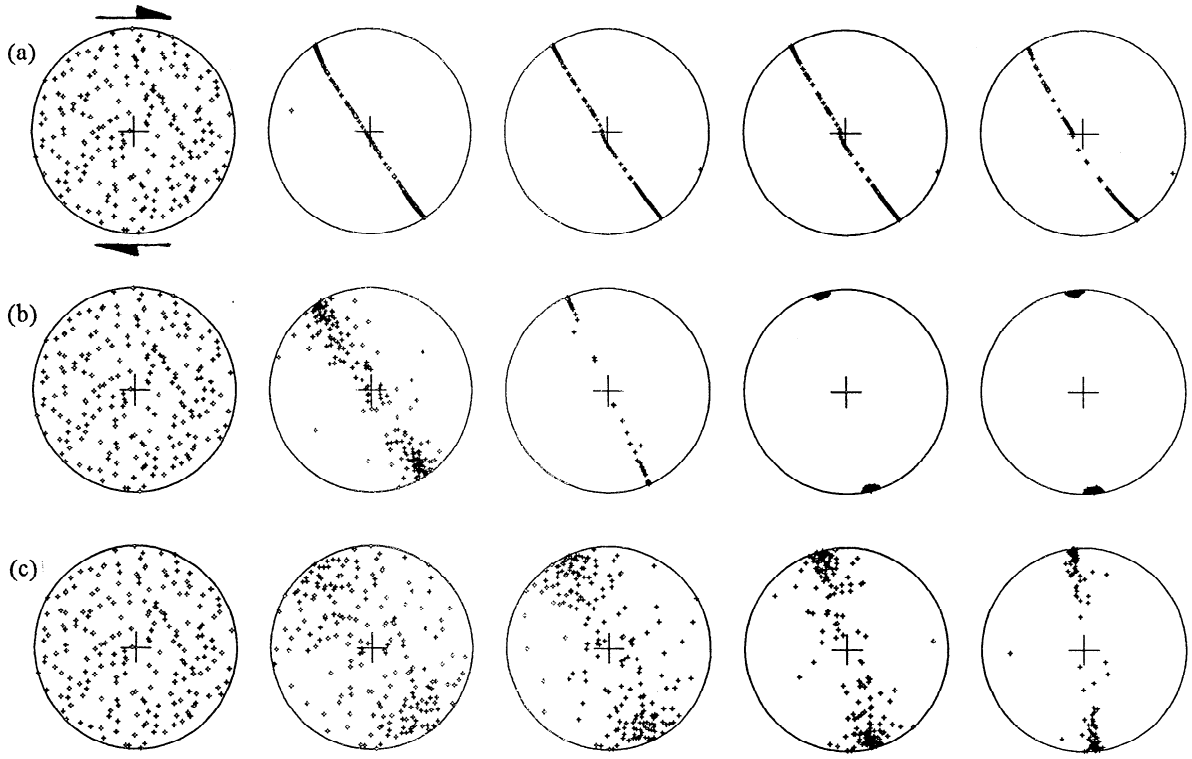

Figure 11. Development of *c* axis fabric in simple shear: (a) static model, (b) VPSC scheme (spherical grains), and (c) Taylor model. Fabrics are given for the initial polycrystal (random orientation), and after equivalent strain of 0.5, 1, 2, and 5.

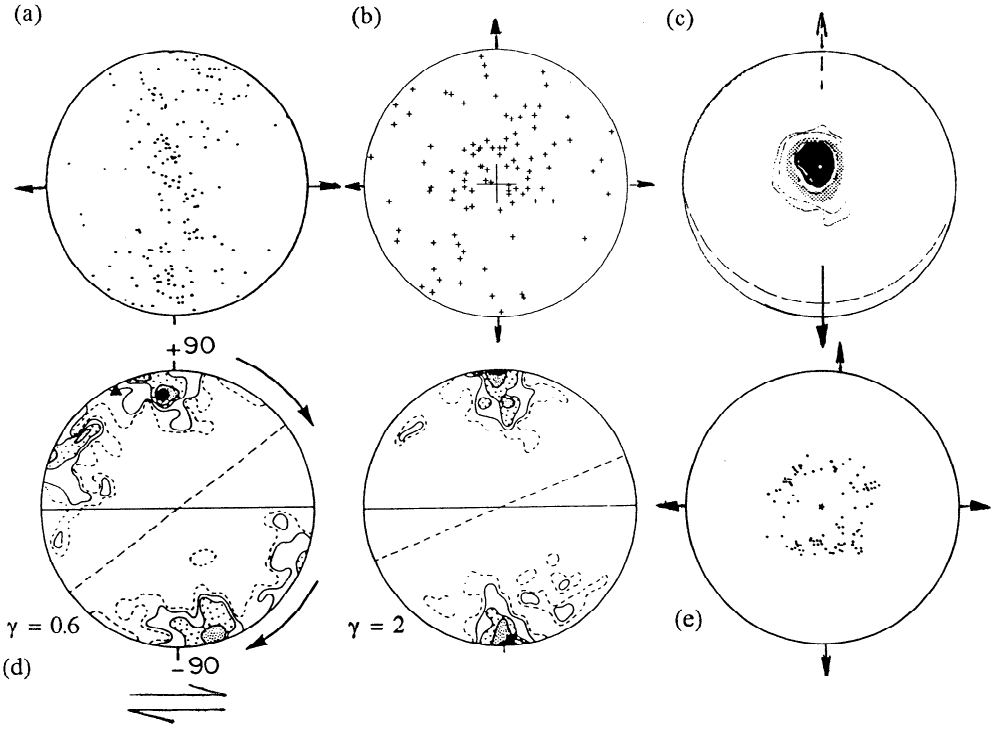

Figure 12. Patterns of *c* axis fabric for natural (Figures 12a to 12c) and artificial (Figures 12d and 12e) ices: (a) Vostok, 915 m deep [*Lipenkov et al.*, 1989]; (b) Dome C, 850 m deep; (c) Byrd, 1570 m deep [*Gow and Williamson*, 1976]; (d) after a torsion test at -10°C, for shear strain of 0.6 and 2 [*Bouchez and Duval*, 1982]; and (e) after a compression test at -3°C, for an equivalent strain of 0.23 [*Jacka and Maccagnan*, 1984]. Equal-area projection. Center of diagrams in Figures 12a to 12c corresponds to the in situ vertical direction.

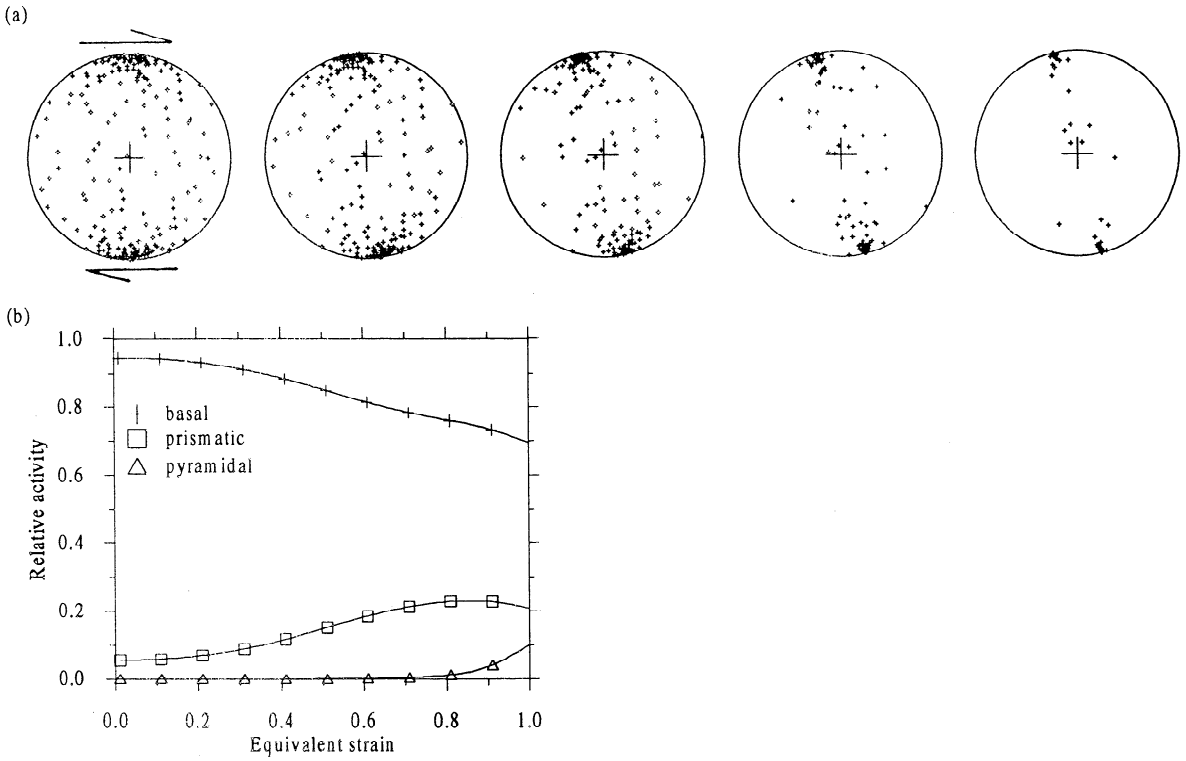

Figure 13. Polycrystal evolution simulated in simple shear with the VPSC model (spherical grains), where the initial polycrystal presents a single maximum fabric. (a) Fabric pattern for the initial polycrystal, and after an equivalent strain of 0.25, 0.5, 0.75, and 1. (b) Activity of basal, prismatic, and pyramidal systems.

shear. This deformation sequence should match natural deformation history more closely. As we can see, the fabric maximum, formed during the compression test, rotates slightly away from its initial position during the shear deformation, and the final fabric clearly compares well with that obtained with an initially isotropic polycrystal. Due to the slight disorientation of the fabric maximum, increasing activity of nonbasal systems is required (Figure 13b).

Thus since an extensive activity of nonbasal systems is not in accordance with observations of dislocations in ice, the static, VPSC, and Taylor models are not able to reproduce realistically simple shear fabrics observed in polar ices. However, these comparisons are limited by the knowledge of the real deformation history of natural ices.

Comparison With Laboratory Experiments

Conditions for fabric development by slip cannot easily be reproduced in the laboratory. Indeed, to avoid excessively long, drawn-out experiments, the level of stress is much higher than that corresponding to in situ conditions, and the temperature is generally higher than -10°C. Dynamic recrystallization with a fast grain boundary migration rate is therefore in most cases a predominant mechanism for fabric development. A typical texture with coarse and interlocking grains is usually observed [*Duval,* 1981].

Fabric development in torsion, under conditions for which migration recrystallization was not readily occurring, was analyzed by *Bouchez and Duval* [1982]. Three samples were deformed for shear strain of 0.6, 0.95, and 2.0 (i.e., equivalent strain of 0.35, 0.55, and 1.15, respectively). Fabrics obtained for shear strain of 0.6 and 2 are shown Figure 12d. The first fabric presents a bimodal distribution of *c* axes. Two maximums are found, which are aligned with the principal direction of compression and with the normal to the macroscopic shear plane. With larger deformation, the first maximum disappears, and most of the basal planes are parallel to the shear plane. This final fabric is similar to that obtained in ice sheets (see Figure 12c) and in shear zones in glaciers [*Huddleston,* 1977]. This fabric development cannot be obtained with the polycrystal models used here. The role of dynamic recrystallization in the fabric development may be invoked.

Comparison With Other Anisotropic Materials

Compared to other materials, the monocrystal of ice is highly anisotropic. Basal slip provides only two independent slip systems, which are not sufficient to satisfy overall compatibility. However, fabric development in polycrystalline ice can be compared with that obtained with other anisotropic materials. Particular attention should be paid to the fabric found in simple shear. Our numerical results show that the easiest slip plane is inclined to the macroscopic shear plane. This is in contradiction with the intuitive preconception widely held in glaciology and geology. However, fabric development similar to that calculated in this study has been found in quartzite [*Wenk et al.,* 1989a], in peridotite [*Chastel et al.,* 1993; *Wenk et al.,* 1991], and in olivine [*Ribe and Yu,* 1991; *Parks and Ahzi,* 1990], as well as in a two-dimensional polycrystalline aggregate with only one slip system [*Zhang et al.,* 1994]. All these studies were performed with polycrystal models in which either the equilibrium conditions, or the compatibility

conditions, or both, were fulfilled. A special fabric development in simple shear was found by *Etchecopar* [1977]. This evolution, in which the secondary maximum of the initial bimodal distribution slowly disappears as deformation proceeds, compares very well with that of *Bouchez and Duval* [1982]. However, within the kinematic polycrystal model of Etchecopar, where only one slip plane has been introduced, very elongated grains are divided into smaller grains in order to make the crystallographic rotation possible.

Evolution of the Polycrystal Strength With Deformation

Let us now compare the polycrystal response predicted by all models as deformation proceeds. The evolution of the normalized equivalent stress $\bar{S}_{eq} / \sigma_0 . \bar{D}_{eq}^{1/3}$ is plotted against the half apex angle θ in Figure 14, for uniaxial deformation. Increasing values of the half apex angle correspond to an extension, and decreasing values correspond to a compression. Furthermore, in uniaxial extension and compression, symmetry axes of fabrics are also principal directions of the macroscopic velocity gradient tensor. As a result, the equivalent stress represents only axial stresses. A general feature of Figure 14 is the increase of the equivalent stress during the deformation. In uniaxial extension the static model predicts a slightly harder polycrystal than the VPSC model. In compression we found the opposite result.

In these calculations, changes in the polycrystal strength with deformation are due only to changes in crystal orientations and not to microstructural hardening. The strength of the polycrystal largely depends on the activity of slip systems. With the static model, since nonbasal systems are not active, an important structural hardening appears when the half apex angle θ is close to 0° in compression and to 90° in extension. With the self-consistent and Taylor models, the increase of the polycrystal strength with deformation is more significant in compression than in extension. This dissymmetry is due only to the necessity of activating pyramidal slip in compression. The normalized stress $\bar{S}_{eq} / \sigma_0 . \bar{D}_{eq}^{1/3}$ predicted by the Taylor model cannot exceed 2.7 in compression and 1.3 in extension, i.e., the corresponding hardening cannot exceed $2.7^3 \approx 20$ and $1.3^3 \approx 2.2$, respectively. The evolution of polycrystal behavior predicted by both VPSC and static models compares well with results from mechanical tests on polar anisotropic ices [*Pimienta and Duval*, 1987], where a normalized stress of at least 2 has been found.

In simple shear, the evolution of the mechanical response as deformation proceeds greatly depends on the models. Indeed, fabric development presents large differences among all models. Since grains rotate first toward hard orientations for basal slip, the polycrystal strength increases. Predicted structural hardening deduced from the VPSC model is of the same order as that obtained in compression and extension. The increase of the equivalent stress with deformation is due to the increase of the activity of nonbasal systems.

Calculations in shear were also made for ices in which the basal plane of all crystals is nearly parallel to the macroscopic shear plane. For a fabric similar to that of the Byrd core at a depth of 1570 m, the equivalent normalized stress predicted with the VPSC model is about 0.45 (i.e., a softening of 11). This result is close to that determined experimentally [*Pimienta and Duval*, 1987]. According to *Castelnau and Duval* [1995], the normalized stress obtained with the lower bound cannot be smaller than 0.6 (i.e., the softening cannot exceed 4.4).

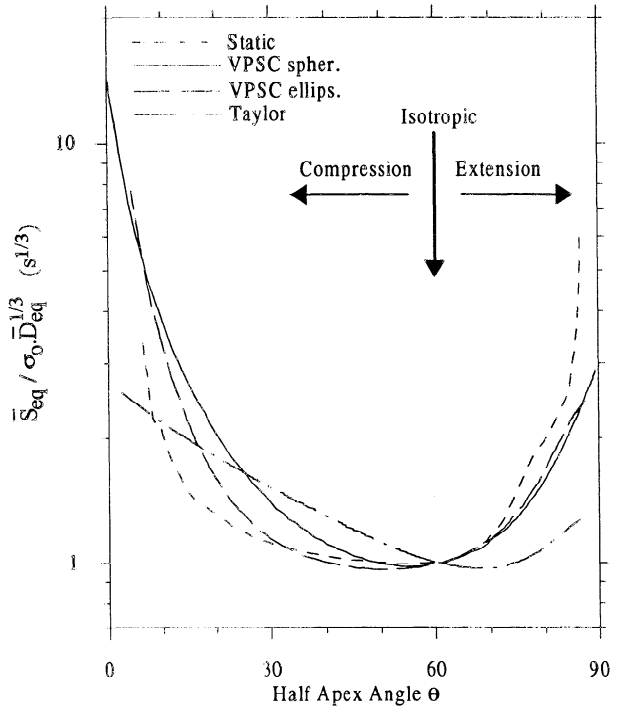

Figure 14. Evolution of the normalized equivalent stress with the half apex angle θ, for uniaxial deformation in extension and compression.

Discussion

We have applied a viscoplastic self-consistent approach to simulate the development of the preferred lattice orientation in ice and to predict the mechanical behavior of anisotropic ices. Results have been compared with those derived from lower and upper bounds. The input parameters for calculations were determined from deformation data on ice monocrystals and isotropic polycrystals. We have shown that the VPSC model is the only one able to predict the viscoplastic response of an isotropic polycrystal on both the microscopic and the macroscopic scale. For large deformation it has been found that natural fabrics obtained in uniaxial extension and compression can be reproduced numerically. The rate of development of fabrics is highly dependent on the interaction relationship. However, the extent of the activity of prismatic and pyramidal slip systems can be questioned. The possibility of determining the dislocation structure in deep Vostok ices should be studied. In simple shear it has been found that the vertical single maximum fabric usually found in deep polar ices (see Figure 12c) can be obtained numerically only with an extensive activation of nonbasal systems. Finally, in the last section, it has been shown that the behavior of anisotropic ices is well described with the self-consistent estimate.

We have shown that a continuous variation from lower bound to upper bound can be obtained by tuning an interaction coefficient (equation (48)). This coefficient α,

introduced by *Molinari and Tóth* [1994], represents the interaction stiffness between grain and matrix.

According to *Hutchinson* [1977], the behavior of a polycrystal of ice is well reproduced with an anisotropic VPSC secant formulation taking $\tau_b = 10\,\tau_a$ and $\tau_c \geq 4\,\tau_b$, which differs slightly from results of the tangent formulation used in this paper. Within the secant formulation, $\underline{\underline{M}}^{(tg)}$ is replaced in (19) by $\underline{\underline{M}}^{(sec)}$. According to (16), both approaches lead to similar results taking $\alpha = 1/N = 1/3$ within the tangent formulation, which has been verified numerically. The secant formulation then lies between the tangent formulation and the Taylor approximation. With the values of RRSS given by relationship (46), the isotropic tangent VPSC model of *Molinari et al.* [1987] predicts $\sigma_o / \tau_a = 6$. This low value can be reproduced with the anisotropic model with $\alpha = 3$. This difference is attributed to the fact that within the isotropic estimation, the strain rate $\underline{D}$ in the HEM is assumed to be nearly proportional to the imposed strain rate $\overline{\underline{D}}$. The polycrystal behavior calculated with isotropic and anisotropic formulations differs by less than 10% only for $\tau_b = \tau_c \leq 3\,\tau_a$. From *Tóth et al.* [1994], results of creep tests a on an isotropic material (mixture of camphor and octachloropropane) lie between tangent and secant formulations of the isotropic VPSC model. A similar conclusion has been given for the response, predicted by the finite element method, of an isotropic spherical inclusion in an isotropic HEM [*Molinari and Tóth*, 1994]. Thus the results obtained with the tangent anisotropic VPSC estimate, presented in previous sections, must be taken only as a first approximation of the real polycrystal response.

The introduction of the interaction coefficient α is valid for small deformation. However, real static (from equation (8)) and VPSC estimates with $\alpha > 100$ do not lead to similar fabric evolution rate, since the rotation rate $\underline{w}^e$ of the associated ellipsoid (equation (23)) is not negligible. Thus a new formulation for this interaction term must be found.

Muguruma [1969] has shown that the surface roughness of a monocrystal significantly influences its mechanical behavior. This is attributed to the possibility for the surface to produce dislocations. Similarly, the dislocation production rate should differ from a free surface and a grain boundary. Thus a reference to the mechanical response of an isolated crystal for the determination of the relative resistance of slip systems of grains within a polycrystal should be reconsidered. For conditions prevailing in ice sheets (deviatoric stress lower than 0.1 MPa), the expected quasi-Newtonian viscosity would result from a constant dislocation density [*Duval et al.*, 1983].

Simulations with the self-consistent model were performed with and without the evolution of the grain shape. It was found that the final fabric pattern is qualitatively similar. However, distorted grain shape slows down the rotation rate of *c* axes, though this effect is significant only after an equivalent strain of about 0.3, i.e. for an aspect ratio of grains of at least 1.5. In polar ice sheets, very elongated grains are found only in ices with a very high impurity content. In pure ice a large elongation is impeded by the effects of grain boundary migration. In the GRIP ices (central Greenland), the aspect ratio of grains ranges between 1.2 and 1.7 for depth between 400 m and 2800 m, with an average value of 1.35 [*T. Thorsteinsson*, personal communication, 1995]. In the Vostok ices, a mean aspect ratio of about 1.5 is observed [*Lipenkov et al.*, 1989]. For a realistic simulation, grain shape effects should be taken into account when the grain boundary migration rate is relatively low.

Deformation by slip and recrystallization are closely linked in polar ices. Both mechanisms influence fabric development [*Alley*, 1992]. When only grain growth occurs, strain energy is low compared with grain boundary surface energy, and fabrics induced by intracrystalline slip strengthen with depth [*Lipenkov et al.*, 1989]. There is therefore no correlation between grain size and crystal orientation. This recrystallization processes should influence the polycrystal behavior and the kinetic of fabric formation only by relaxing the field of internal stress, to make the stress more uniform within the polycrystal.

With rotation recrystallization, fabric is essentially the result of lattice rotation by dislocation glide. However, the grain boundary migration, the progressive disorientation of subboundaries, and the nucleation of new strain-free grains can be mechanisms which alter the fabric development. The progressive misorientation of subboundaries tends to produce less concentrated fabrics [*Castelnau et al.*, 1996]. Nucleation occurs in grains where there is a curvature of the lattice by bending moments. From *Wilson* [1986], kink bands form in grains oriented with their basal plane more or less parallel to the shortening direction. According to Figure 6, grains badly oriented for basal glide are more stressed. Due to the interaction between neighbor grains, the deformation of these grains must be very heterogeneous [*Wilson and Zhang*, 1994]. Moreover, the subgrain size is inversely proportional to the the applied stress [*Poirier*, 1985]. Thus badly oriented grains should contain more subboundaries and smaller subgrains. These grains should have a high level of stored energy, associated with a large amount of subboundaries. Thus grains well oriented for basal slip are favored for growth. However, this mechanism is progressive, since the misorientation between new and parent grains is typically 15° [*Poirier*, 1985]. On the other hand, owing to the low grain boundary migration rate, rotation recrystallization is generally not enough efficient to control fabric development [*Duval and Castelnau*, 1995]. A special case is found for simple shear [*Kamb*, 1972; *Bouchez and Duval*, 1982]. As was shown previously, the fabric development simulated in simple shear does not match observations on natural ices. A possibility is that due to the relatively large shear rate, as is usually found in the deeper parts of ice sheets, the stored strain energy contributes significantly to the total driving force for grain boundary migration. The preferential growth of grains well oriented for basal glide (i. e., with a vertical *c* axis) could be associated with lattice rotation by slip to produce the vertical single maximum usually observed in ice sheets.

When migration recrystallization occurs, the grain boundary migration rate is about 2 orders of magnitude higher than during grain growth and rotation recrystallization. A complete recrystallization cycle is obtained for a strain between 3% and 5% [*Steineman*, 1954]. As a result, the fabric reflects the instantaneous stress state and not the kinematic framework. Migration recrystallization produces fabrics favorable to basal slip [*Duval*, 1981]. This effect is clearly illustrated in compression and extension. In the laboratory experiments of *Jacka and Maccagnan* [1984], ice samples deformed at -3°C in compression develop circle girdle fabrics around the compression axis (Figure 12e). The mean half angle of fabrics depends on the accumulated strain

but is generally close to 30°. With these fabric patterns, grains are well oriented for basal glide. A structural hardening, associated with *c* axes close to the compression axis, is then obtained only when this recrystallization regime is not dominant. Typical fabrics induced by migration recrystallization are found in temperate glaciers and in polar ice sheets near the bedrock [*Gow and Williamson*, 1976; *Vallon et al.*, 1976].

In this study, large differences between predictions of both lower and upper bounds and the VPSC theory were obtained. The introduction in the VPSC model of the nucleation of grains and of grain boundary migration associated with grain growth, rotation recrystallization, and migration recrystallization should greatly improve simulations for fabric development in polar ices. The interaction between the inclusion and the HEM can be modulated by a tuning parameter to take into account the accommodation of slip by the grain boundary migration. This possibility will be investigated to improve the simulation of fabric development in polar ices.

Acknowledgments. This work was supported by PNEDC (Programme National d'Etudes de la Dynamique du Climat) CNRS, France, and by the CEC (Commission of European Communities) Environment Programme.

References

Ahmad, S., and R. W. Whitworth, Dislocation motion in ice: A study by synchroton X-ray topography, *Philos. Mag. A, 57* (5), 749-766, 1988.

Alley, R. B., Fabrics in polar ice sheets: Development and prediction, *Science, 240*, 4851, 493-495, 1988.

Alley, R. B., Flow-law hypotheses for ice-sheet modeling, *J. Glaciol., 38* (129), 245-256, 1992.

Alley, R. B., A. J. Gow, and D. A. Meese, Mapping *c*-axis fabrics to study physical processes in ice, *J. Glaciol., 41* (137), 197-203, 1995.

Azuma, N., A flow law for anisotropic ice and its application to ice sheets, *Earth Planet. Sci. Lett., 128*, 601-614, 1994.

Azuma, N., A flow law for anisotropic polycrystalline ice under uniaxial compressive deformation, *Cold Reg. Sci. Technol., 23*, 137-147, 1995.

Azuma, N. and A. Higashi, Formation processes of ice fabric pattern in ice sheets, *Ann. Glaciol., 6*, 130-134, 1985.

Barber, D. J., H.-R. Wenk, and H. C. Heard, The plastic deformation of polycrystalline dolomite: Comparison of experimental results with theoretical predictions, *Mater. Sci. Eng. A, 175*, 83-104, 1994.

Becker, R., and S. Panchanadeswaran, Effects of grain interactions on deformation and local texture in polycrystals, *Acta Metall. Mater., 43* (7), 2701-2719, 1995.

Bouchez, J. L., and P. Duval, The fabric of polycrystalline ice deformed in simple shear: Experiments in torsion, natural deformation and geometrical interpretation, *Textures Microstruct., 5*, 171-190, 1982.

Budd, W. F., and T. H. Jacka, A review of ice rheology for ice sheet modelling, *Cold Reg. Sci. Technol., 16*, 107-144, 1989.

Canova, G. R., H. R. Wenk, and A. Molinari, Deformation modelling of multi-phase polycrystals: Case of a quartz-mica aggregate, *Acta Metall. Mater., 40* (7), 1519-1530, 1992.

Castelnau, O., and P. Duval, Simulations of anisotropy and fabric development in polar ices, *Ann. Glaciol., 20*, 277-282, 1995.

Castelnau, O., T. Thorsteinsson, J. Kipfstuhl, P. Duval, and G. R. Canova, Modelling fabric development along the GRIP ice core (central Greenland), *Ann. Glaciol., 23*, in press, 1996.

Chastel, Y. B., P. R. Dawson, H.-R. Wenk, and K. Bennett, Anisotropic convection with implications for the upper mantle, *J. Geophys. Res., 98* (B10), 17757-17771, 1993.

Doake, C. S. M., and E. W. Wolff, Flow law for ice in polar ice sheets, *Nature, 314*, 255-257, 1985.

Duval, P., Lois du fluage transitoire ou permanent de la glace polycrystalline pour divers états de contrainte, *Ann. Géophys. 32*, 335-350, 1976.

Duval, P., Creep and fabrics of polycrystalline ice under shear and compression, *J. Glaciol., 27* (95), 129-140, 1981.

Duval, P., and O. Castelnau, Dynamic recrystallization of ice in polar ice sheets, *J. Phys. IV (suppl. J. Phys. III), C3*, 5, 197-205, 1995.

Duval, P., and H. Le Gac, Mechanical behavior of antarctic ice, *Ann. Glaciol., 3*, 92-95, 1982.

Duval, P., M. F. Ashby, and I. Anderman, Rate-controlling processes in the creep of polycrystalline ice, *J. Phys. Chem., 87* (21), 4066-4074, 1983.

Etchecopar, A., A plane kinematic model of progressive deformation in a polycrystalline aggregate, *Tectonophysics, 39*, 121-139, 1977.

Eshelby, J. D., The determination of the elastic field of an ellipsoidal inclusion, and related problems, *Proc. R. Soc. London, A, 241*, 376-396, 1957.

Fujita, S., M. Nakawo, and S. Mae, Orientation of the 700-m Mizuho core and its strain history, *in Proceeding, NIPR Symposium on Polar Meteorology and Glaciology*, vol. 1, 122-131, Tokyo, Japan, 1987.

Fukuda, A., T. Hondoh, and A. Higashi, Dislocation mechanisms of plastic deformation of ice, *J. Phys. (suppl. J. Phys III), C1*, 48, 163-173, 1987.

Gow, A. J., and T. Williamson, Rheological implications of the internal structure and crystal fabrics of the West Antarctic ice sheet as revealed by deep core drilling at Byrd Station, *CRREL Rep. 76-35*, U.S. Army Cold Reg. Res. and Eng. Lab., Hanover, N.H., 1976.

Guillopé, M., and J. P. Poirier, Dynamic recrystallization during creep of single-crystalline halite: An experimental study, *J. Geophys. Res., 84* (B10), 5557-5567, 1979.

Gundestrup, N. S., and B. L. Hansen, Bore-hole survey at Dye 3, South Greenland, *J. Glaciol., 30* (106), 282-288, 1984.

Higashi, A., A. Fukuda, T. Hondoh, K. Goto, and S. Amakai, Dynamical dislocation processes in ice crystal, *Proceeding of the Yamada Conference IX on Dislocations in Solids*, edited by T. Suzuki, T. Ninomiya, K. Sumino, and S. Takeuchi, 511-515, Univ. of Tokyo Press, Tokyo, 1985.

Hill, R., Continuum micro-mechanics of elastoplastic polycrystals, *J. Mech. Phys. Solids, 13*, 89-101, 1965.

Hondoh, T., H. Iwamatsu, and S. Mae, Dislocation mobility for nonbasal glide in ice measured by in situ X-ray topography, *Philos. Mag. A, 62* (1), 89-102, 1990.

Hooke, R. L., Flow law for polycrystalline ice glaciers: Comparison of theoretical predictions, laboratory data, and field measurements, *Rev. Geophys., 19* (4), 664-672, 1981.

Huddleston, P. J., Progressive deformation and development of fabrics across zones of shear in glacial ice, in *Energetics of Geological Processes*, edited by S. K. Saxena and S. Bhattacharji, pp. 121-150, Springer-Verlag, New York, 1977.

Hutchinson, J. W., Bounds and self-consistent estimates for creep of polycrystalline materials, *Proc. R. Soc. London, A, 348*, 101-127, 1976.

Hutchinson, J. W., Creep and plasticity of hexagonal polycrystals as related to single crystal slip, *Metall. Trans. A, 8* (9), 1465-1469, 1977.

Jacka, T. H., The time and strain required for development of minimum strain rates in ice, *Cold Reg. Sci. Technol., 8*, 261-268, 1984.

Jacka, T. H., and M. Maccagnan, Ice crystallographic and strain rate changes with strain in compression and extension, *Cold Reg. Sci. Technol., 8*, 269-286, 1984.

Kamb, W. B., The glide direction in ice, *J. Glaciol., 3* (30), 1097-1106, 1961.

Kamb, W. B., Experimental recrystallization of ice under stress, in *Flow and Fracture of Rocks, Geophys. Monogr. Ser.*, vol. 16, edited by H. C. Heard, Y. Borg, N. L. Carter, and C. B. Raleigh, pp. 211-241, AGU, Washington, D.C., 1972.

Kocks, U. F., The relation between polycrystal deformation and single crystal deformation, *Metall. Trans., 1*, 1121-1143, 1970.

Lebensohn, R. A., and C. N. Tomé, A self-consistent anisotropic approach for the simulation of plastic deformation and texture development of polycrystals: Application to zirconium alloys, *Acta Metall., 41*, 2611-2624, 1993.

Lebensohn, R. A., and C. N. Tomé, A self-consistent viscoplastic model: Prediction of rolling textures of anisotropic polycrystals, *Mater. Sci. Eng. A, 175*, 71-82, 1994.

Lebensohn, R. A., P. V. Sanchez, and A. A. Pochettino, Modelling texture development of zirconium alloys at high temperatures, *Scr. Metall. Mater., 30*, 481-486, 1994.

Lipenkov, V. Ya., N. I. Barkov, P. Duval, and P. Pimienta, Crystalline texture of the 2083-m ice core at Vostok station, Antarctica, *J. Glaciol., 35* (121), 392-398, 1989.

Lliboutry, L., and P. Duval, Various isotropic and anisotropic ices found in glaciers and polar ice caps and their corresponding rheologies, *Ann. Geophys., 3* (2), 207-224, 1985.

Molinari, A., and L. S. Tóth, Tuning a self-consistent viscoplastic model by finite element results, I, modeling, *Acta Metall. Mater., 42* (7), 2453-2458, 1994.

Molinari, A, G. R. Canova, and S. Ahzy, A self-consistent approach of the large deformation polycrystal viscoplasticity, *Acta Metall., 35* (12), 2983-2994, 1987.

Muguruma, J., Effects of surface condition on the mechanical properties of ice crystals, *Br. J. Appl. Phys., 2* (2), 1517-1525, 1969.

Parks, D. M., and S. Ahzi, Polycrystalline plastic deformation and texture evolution for crystals lacking five independent slip systems, *J. Mech. Phys. Solids, 38* (5), 701-724, 1990.

Pimienta, P., and P. Duval, Mechanical behavior of anisotropic polar ice, in *The Physical Basis of Ice Sheet Modelling, International Association of Hydrological Sciences Publ. 170,* 57-66, 1987.

Pimienta, P., and P. Duval, Rheology of polar glacier ice (abstract), *Ann. Glaciol., 12*, 206, 1989.

Poirier, J. P., *Creep of Crystals*, Cambridge Univ. Press, New York, 1985.

Ribe, N. M., and Y. Yu, A theory for plastic deformation and textural evolution of olivine polycrystals, *J. Geophys. Res., 96* (B5), 8325-8335, 1991.

Russell-Head, D. S., and W. F. Budd, Ice-flow properties derived from bore-hole shear measurement combined with ice-core studies, *J. Glaciol., 24* (90), 117-130, 1979.

Sachs, G., Zur Ableitung einer Fliessbedingung, *Z. Ver. Dtsch. Ing., 72*, 734-736, 1928.

Shearwood, C., and R. W. Whitworth, Novel processes of dislocation multiplication observed in ice, *Acta Metall. Mater., 41* (1), 205-210, 1993.

Shoji, H., and C. C. Langway, Flow-law parameters of the Dye 3, Greenland, deep ice core, *Ann. Glaciol., 10,* 146-150, 1988.

Steineman, S., Flow and recrystallization of ice, *IAHS Publ., 39,* 449-462, 1954.

Taylor, G. I., Plastic strain in metals, *J. Inst. Met., 62*, 307-324, 1938.

Tomé, C. N., H.-R. Wenk, G. R. Canova, and U. F. Kocks, Simulation of texture development in calcite: Comparison of polycrystal plasticity theories, *J. Geophys. Res., 96* (B7), 11,865-11,875, 1991.

Tóth, L. S., A. Molinari, and P. D. Bons, Self consistent modelling of the creep behavior of mixtures of camphor and octachloropropane, *Mater. Sci. Eng. A, 175,* 231-236, 1994.

Vallon, M., J.-R. Petit, and B. Fabre, Study of an ice core to the bedrock in the accumulation zone of an alpine glacier, *J. Glaciol., 17,* 13-28, 1976.

Van der Veen, C. J., and I. M. Whillans, Development of fabric in ice, *Cold Reg. Sci. Technol., 22,* 171-195, 1994.

Wang, J. N., Harper-Dorn creep in olivine, *Mater. Sci. Eng. A, 183,* 267-272, 1994.

Wei, Y., and J. P. Dempsey, The motion of nonbasal dislocation in ice crystals, *Philos. Mag. A, 69* (1), 1-10, 1994.

Wenk, H.-R., T. Takeshita, P. Van Houtte, and F. Wagner, Plastic anisotropy and texture development in calcite polycrystal, *J. Geophys. Res., 91* (B3), 3861-3869, 1986.

Wenk, H.-R., G. R. Canova, A. Molinari, and U. F. Kocks, Viscoplastic modelling of texture development in quartzite, *J. Geophys. Res., 94* (B12), 17,895-17,906, 1989a.

Wenk, H.-R., G. R. Canova, A. Molinari, and H. Mecking, Texture development in halite: Comparison of Taylor model and self-consistent theory, *Acta Metall., 37* (7), 2017-2029, 1989b.

Wenk, H.-R., K. Bennett, G. R. Canova, and A. Molinari, Modelling plastic deformation of peridotite with the self-consistent theory, *J. Geophys. Res., 96* (B5), 8337-8349, 1991.

Wilson, C. J. L., Deformation induced recrystallization of ice: The application of in situ experiments, in *Mineral and Rock Deformation: Laboratories Studies, Geophysical Monogr. Ser., vol. 36,* edited by B.E. Hobbs and H.C. Heard, pp. 213-232, AGU, Washington, D.C., 1986.

Wilson, C. J. L., and Y. Zhang, Comparison between experiment and computer modelling of plane-strain simple-shear ice deformation, *J. Glaciol., 40* (134), 46-55, 1994.

Zhang, Y., B. E. Hobbs, and A. Ord, A numerical simulation of fabric development in polycrystalline aggregates with one slip system, *J. Struct. Geol., 16* (9), 1297-1313, 1994.

G. R. Canova, Laboratoire de Génie Physique et Mécanique des Matériaux, Ecole Nationale Supérieure de Physique de Grenoble, rue de la physique, BP 96, 38402 St.-Martin D'Hères, France. (e-mail: gilles@gpm2.grenet.fr)

O. Castelnau and P. Duval, Laboratoire de Glaciologie et Géophysique de l'Environnement, CNRS, rue Molière, BP 96, 38402 St.-Martin d'Hères, France. (e-mail: olivier@glaciog.grenet.fr; duval@glaciog.grenet.fr)

R. A. Lebensohn, Instituto de Física de Rosario, Consejo Nacional de Invastigaciones Científicas y Tecnicas, Universidad Nacional de Rosario, 27 de febrero 210 bis, 2000 Rosario, Argentina. (e-mail: ricardo@ifir.edu.ar)

(Received May 8, 1995; revised January 4, 1996;
accepted January 30, 1996.)